

**A STUDY OF THE SECONDARY ORGANIC AEROSOL
FORMATION POTENTIALS OF IMPORTANT
COMPOUNDS IN THE ATMOSPHERE**

Final Report

CRC Project No. A-41

Submitted by:

**James F. Pankow, William E. Asher,
Robert J. Griffin, and John H. Seinfeld**

August 2003



**Coordinating Research Council, Inc.
3650 Mansell Road, Suite 140 - Alpharetta, Georgia 30022**

A STUDY OF THE SECONDARY ORGANIC AEROSOL FORMATION POTENTIALS OF IMPORTANT COMPOUNDS IN THE ATMOSPHERE

Final Report

CRC Project No. A-41

Submitted by:

**James F. Pankow¹, William E. Asher^{1,2},
Robert J. Griffin³, and John H. Seinfeld⁴**

August 2003

¹Department of Environmental and Biomolecular Systems, OCI School of Science & Engineering, Oregon Health & Science University, Portland, OR 97291, Tel: 503-748-1080

²Applied Physics Laboratory, University of Washington, Seattle, WA 98195, Tel: 206-543-5942

³EOS/Earth Sciences, 357 Morse Hall, 39 College Road, University of New Hampshire, Durham, NH, 03824, Tel: 603-862-2021

⁴Department of Chemical Engineering, California Institute of Technology, Mail Code 210-41, Pasadena, California 91125, Tel: 626-395-4635

Disclaimer

This report was prepared by the Oregon Health & Science University as an account of work sponsored by the Coordinating Research Council (CRC) with additional support from the American Chemistry Council (ACC). Neither the CRC, members of the CRC, the ACC, members of ACC, nor any person acting on their behalf: (1) makes any warranty, express or implied, with respect to the use of any information, apparatus, method, or process disclosed in this report, or (2) assumes any liabilities with respect to use of, inability to use, or damages resulting from the use or inability to use, any information, apparatus, method, or process disclosed in this report.

Table of Contents

	<u>page</u>
Disclaimer	2
1. Executive Summary	4
2. Background	5
2.1. The SOA Yield (Y)	5
2.2. The Differential Organic Particulate Matter Formation Potential (θ_{OPM})	5
2.3. Predicting the Products of VOC Oxidation	6
3. Research Results	8
3.1. Task 1: Study Compounds	8
3.1.1. Selected Parent VOCs and Reaction Pathways	8
3.1.2. Levels of Condensable SOCs From Primary Emissions	10
3.2. Task 2: Simulations	12
3.2.1. Base & Sensitivity Cases	12
3.2.2. Model Components of OPMBOX	14
3.2.2.1. The Chemical Kinetics Model	14
3.2.2.1.1. Description	14
3.2.2.1.2. General Applicability	18
3.2.2.2. The OPM Formation Model	18
3.3. Task 3: OPM Formation Results for Illustrative Conditions of Interest	24
3.3.1. OPM Formation in the Absence of Condensable Primary Emissions	24
3.3.2. Task 3.2: Effect of Condensable Primary Emissions on Aerosol Mass	27
3.4 Task 4. Implications of the Study for Laboratory Chamber Experiments	28
4. References	31
5. List of Figures	34

1. Executive Summary

Organic particulate matter (OPM) is known to form in the atmosphere as a consequence of the oxidation of parent volatile organic compounds (VOCs). The concept of the **differential organic particulate matter (OPM) formation potential (θ_{OPM})** is defined as the condition-dependent rate of change in OPM formation with increases in $\text{VOC}_{i,\text{init}}$, the initial concentration of a specific VOC i . $\theta_{\text{OPM},i}$ gives the slope according to which M_o changes as $\text{VOC}_{i,\text{init}}$ increases. The view in the field of atmospheric chemistry is that increases in VOC emissions generally lead to increases in OPM formation. However, there does remain the possibility that in some special systems, some increases in VOC emissions could lead to changes in ozone chemistry etc. that lead to decreases in OPM formation. A model was constructed to allow the prediction of θ_{OPM} values under a wide range of conditions for a set of atmospherically-important VOCs. The model links a gas-phase chemical kinetics component with a gas/particle condensation component, and allows prediction of the mass concentration of OPM ($= M_o, \mu\text{g}/\text{m}^3$) as a function of time, oxidant, and VOC levels. Multiple example cases are discussed. The effects of condensable primary emissions on M_o levels are also considered. The greatest uncertainty in predicting OPM formation lies in understanding the pathways and kinetics of the VOC oxidation reactions. The implications of the study for laboratory chamber experiments are also discussed.

2. Background

2.1. SOA Yield (Y)

The often-discussed **fractional mass yield** Y , which has been used to describe the aggregate amount of SOA that is produced when a certain amount of a parent gaseous VOC is oxidized to condensable products. Y is defined as

$$Y = \frac{\Delta M_o}{\Delta \text{VOC}} \quad (1)$$

where ΔM_o ($\mu\text{g m}^{-3}$) is the total mass concentration of organic particulate matter (OPM) produced from the reaction of ΔVOC ($\mu\text{g m}^{-3}$) worth of gaseous VOC. Equation 1 shows that Y values increase as ΔM_o increases, but a more subtle dependence is that between ΔM_o and the fraction of each reaction product that condenses. Specifically, increasing the mass concentration of the SOA phase tends to pull more of each condensable product into that phase. The nature of the dependence of Y on the multiple oxidation products that may form can be parameterized using the matrix approach of Pankow (1994b) and Pankow *et al.* (2001), or by application of the reduced two-product version of that model described by Odum *et al.* (1996) in which four bulk (*i.e.*, averaged) parameters (two mass-based stoichiometric factors and two partition coefficients) are used to fit laboratory yield data.

Values of Y indicate the efficiency with which oxidation products condense **after** those condensable products have actually formed. That is, a Y value relates ΔM_o , the mass concentration of SOA that has formed, to the amount of VOC that has already reacted and gone on to form condensable products.

2.2. The Differential Organic Particulate Matter Formation Potential (θ_{OPM})

Air quality regulators concerned with emissions and managing airsheds are interested in the **potential** of a given additional concentration of VOC to form added SOA, **before** the VOC actually reacts in the atmosphere. Thus, in analogy with the concept of a photochemical ozone

formation potential for VOCs (Derwent *et al.*, 1998), we here define $\theta_{\text{OPM},i}$ as the **Differential OPM Formation Potential** of VOC i :

$$\theta_{\text{OPM},i} = f(\text{VOC}_{i,\text{init}}, \text{VOC}_{j,\text{init}}, M_{\text{o,init}}, [\text{O}_3], [\text{OH}\cdot], [\text{NO}_x], \text{RH}, T, t) = \frac{\partial M_{\text{o}}}{\partial \text{VOC}_{i,\text{init}}} \quad (2)$$

where $\theta_{\text{OPM},i}$ is a very complex function of

$\text{VOC}_{i,\text{init}}$ ($\mu\text{g}/\text{m}^3$):	the initial concentration of VOC_i ;
$\text{VOC}_{j,\text{init}}$ ($\mu\text{g}/\text{m}^3$):	the initial concentrations of all other reacting VOC_j ;
$M_{\text{o,init}}$ ($\mu\text{g}/\text{m}^3$):	the initial concentration of organic PM;
$[\text{O}_3]$, $[\text{OH}\cdot]$, $[\text{NO}_x]$:	time-dependent concentrations of O_3 , $\text{OH}\cdot$, NO_x ;
RH:	relative humidity;
T :	temperature; and
t :	reaction time.

In words, $\theta_{\text{OPM},i}$ (with units of $\mu\text{g}/\text{m}^3$ per $\mu\text{g}/\text{m}^3$) gives the slope according to which M_{o} changes as $\text{VOC}_{i,\text{init}}$ increases (see also discussion in Executive Summary). We reiterate that $\theta_{\text{OPM},i}$ depends on the reaction time. The θ_{OPM} approach can be used to distinguish a VOC that has little potential to form OPM from one that has considerable potential to form OPM.

In this report, we usually refer to the PM of interest as “OPM”, rather than as “SOA”. The reason is that the condensation of **secondary** organic oxidation products can lead to the additional condensation of gaseous compounds of **primary** origin. Thus, in a given circumstance, one may well be interested in how much additional **total** OPM forms due to the presence of VOC_i , and not just the portion of the PM that is condensed secondary oxidation products from the parent hydrocarbon that is VOC_i .

2.3. Predicting the Products of VOC Oxidation

Given the considerable advances that have been made in modeling the condensation formation of OPM, the main remaining obstacle in predicting OPM formation potentials in urban and regional atmospheres is the serious lack of detailed knowledge that exists regarding VOC

oxidation products, namely their molecular structures (or even their approximate structures), their formation stoichiometries relative to their parent VOCs, and their reaction formation kinetics (including the dependence of those compound-dependent kinetics on the ambient chemistry). Unfortunately, reliable laboratory or chamber data of this type are neither easily obtainable, nor likely to soon become available for all of the parent VOCs and reaction chemistries of interest.

An attractive alternative/supplement to comprehensive laboratory and chamber experiments is provided by gas-phase mechanism models that can be used to predict the needs of the OPM formation model, namely general **product structure, formation stoichiometries, and reaction kinetics**. Indeed, Griffin *et al.* (2002) have recently described a gas-phase atmospheric chemical mechanism approach that represents ozone (O₃) chemistry and the consequent formation of individual, condensable organic oxidation products; this is the approach that has been used in this work.

3. Research Results

3.1. Task 1: Study Compounds

3.1.1. Selected Parent VOCs and Reaction Pathways

35 VOCs of interest were selected as being of particular interest for the work conducted here (Table 1). These compounds were selected based on published emission information, state environmental website data, and their observed ambient concentrations in six prototype semi-rural and urban areas that included the Northeast United States, the Southeast United States, Houston, the South Coast Air Basin (SoCAB) of California, the Upper Midwest of the United States, and the United Kingdom (Pankow *et al.*, 2003; Tanaka *et al.*, 2000; Derwent *et al.*, 1998; Aneja *et al.*, 1996; Goldan *et al.*, 1995). Typical ambient concentration ranges were assembled for all 35 compounds. Each of the 35 VOCs can be classified into one of three groups:

- “Ar” Aromatic;
- “A” Aliphatic or Alicyclic;
- “B” Biogenic.

Because of the enormous chemical and computational complexities associated with modeling the detailed formation of products from 35 individual

parent VOCs, ten special study compounds (see Table 1, and Figure 1) were selected from the list of 35 for the actual modeling studies. The ten were chosen based on their importance within

Table 1. 35 VOCs Selected for Emphasis in this Study. (10 Special Study Compounds are Given in Bold.)

<u>VOC</u>	<u>class</u>
4-methyl-1-pentene	A
<i>n</i> -hexane	A
2-hexene	A
cyclohexane	A
2-methylhexane	A
<i>n</i> -heptane	A
<i>n</i> -octane	A
<i>n</i>-decane	A
toluene	Ar
ethylbenzene	Ar
styrene	Ar
<i>m</i>-xylene	Ar
<i>o</i> -xylene	Ar
<i>p</i> -xylene	Ar
<i>o</i> -ethyltoluene	Ar
<i>m</i>-ethyltoluene	Ar
<i>p</i> -ethyltoluene	Ar
<i>n</i> -propylbenzene	Ar
<i>i</i> -propylbenzene	Ar
1,2,3-trimethylbenzene	Ar
1,2,4-trimethylbenzene	Ar
1,3,5-trimethylbenzene	Ar
1,2,3,4-tetramethylbenzene	Ar
1,2,3,5-tetramethylbenzene	Ar
1,2,4,5-tetramethylbenzene	Ar
1-isopropyl-4-methylbenzene	Ar
<i>m</i> -diethylbenzene	Ar
<i>p</i> -diethylbenzene	Ar
<i>n</i> -butylbenzene	Ar
1,2-diethyl-5-methylbenzene	Ar
1,3-diethyl-5-methylbenzene	Ar
naphthalene	Ar
anthracene	Ar
α-pinene	B
β -pinene	B

their compound class, and within its corresponding set of isomers (*e.g.*, among the trimethylbenzene isomers, 1,2,4-trimethylbenzene typically has the highest average observed mixing ratio). In order that the modeling with the 10 compounds would still reflect the overall VOC levels of typical atmospheres of interest, the base case mixing ratios of the 10 compounds were selected by multiplying their typical values so that after this “boosting”, the mixing ratios of the 10 specifically-modeled compounds would represent lumped aggregate concentrations of the broader mix of 35. The specifics of this boosting process as well as the assumed reaction pathways of the ten compounds are discussed below.

Because of the central role that the concentration of the hydroxyl radical ([OH]) plays in atmospheric oxidation of VOCs, it was considered critical that the model accurately predict atmospheric [OH] levels. Smog chamber studies by Odum *et al.* (1996) and Griffin *et al.* (1999) of OPM formation from the gas-phase oxidation of a limited number of starting VOCs have shown that [OH] in smog chambers is significantly smaller than daytime atmospheric [OH]. In experiments such as those carried out by Odum *et al.* (1996) and Griffin *et al.* (1999a), propene (C₃H₆) is added as an additional VOC to raise OH levels without significantly influencing the total amount of OPM formed.

In agreement with the above-mentioned smog chamber studies, [OH] predicted by this chemical model, which also uses a limited set of starting VOCs, was low compared to typical daytime atmospheric [OH]. It was necessary to add propene to the set of VOCs so that [OH] levels predicted by the model agree with atmospheric levels. The total amount of propene used in each simulation was a function of the concentration of decane, 2-methylhexane, cyclohexane, toluene, ethyl toluene, and naphthalene according to the relationship

$$[\text{propene}] = [\text{decane}]/1.1 + ([\text{2-methylhexane}] + [\text{cyclohexane}])/2.1 + [\text{toluene}]/2.5 + ([\text{ethyltoluene}] + [\text{naphthalene}])/4.0 \quad (3)$$

where the divisors 1.1, 2.1, 2.5, and 4.0 were chosen so that if only that compound were present as a parent VOC, then [OH] would be at least 1×10^6 molecules cm^{-3} after several hours of reaction time. Typically, OH concentrations for the simulations described below in Section 3.2 were in the range of $2 - 8 \times 10^6$ molecules cm^{-3} .

3.1.2. Levels of Condensable SOCs From Primary Emissions

Modeling the effects of condensable primary emissions (CPEs) on overall OPM formation requires knowledge of both their resultant mass concentrations and their chemical structures. In most urban airsheds in North America, most of the primary emissions of condensable semi-volatile organic compounds (SOCs) mass are due to emissions from motor vehicles (Schauer *et al.*, 2002). In some cases there can also be significant sources of SOCs from wood smoke. Although the chemical composition of primary SOC emissions is complex, for the purposes of this study they were modeled as cycloparaffinic material from lubrication oils, with varying molecular weight (MW) values in the range of 250 to 500 g/mol.

Total atmospheric levels of the CPEs were based on values measured in Azusa, California (a site just downwind of the Los Angeles Basin) on Sept. 8-9, 1993 (Schauer *et al.*, 2002). In order to adjust these levels for the different cases run for this study, scaling was based on the total initial concentration of toluene in a particular simulation. Toluene is considered the key tracer species for the types of airsheds modeled in this study because it is relatively non-reactive, and Harley *et al.* (1992) have concluded that 50% of the total toluene emissions in the Los Angeles Basin are due to motor vehicles. The total mass concentration of the CPEs were distributed according to MW based on the data for total particulate organic carbon (OC) mass as a function of MW as measured by Fraser *et al.* (1997). Fraser *et al.* (1997) separated the particulate OC into 18 separate MW ranges from 250 to 560 g/mol. In order to simplify the modeling and because there is no difference in general structure within the cycloparaffins (other

than MW), a subset of five MW values spanning the range measured was selected for use. This subset included C₁₈, C₂₂, C₂₆, C₂₉, and C₃₇ with MW values of 246, 300, 354, 390, and 500 g/mol, respectively. The fraction of the total CPE for each of the five MW values was selected based on the data of Fraser *et al.* (1997). In particular: 1) the fraction of CPE mass represented by C₁₈ was estimated by summing the fractions in the MW range 250 to 285 g/mol; 2) the C₂₂ fraction was based on the MW range 300 to 345 g/mol; 3) the C₂₆ fraction was based on the MW range 360 to 380 g/mol; 4) the C₂₉ fraction was based on the MW range 400 to 490 g/mol; and 5) the C₃₇ fraction was based on the MW range 500 to 560 g/mol. Table 2 gives the resulting values and the liquid vapor pressure values as estimated by the method of Asher *et al.* (2001) for the simulation temperature of 298 K.

Table 2. Distribution and Physical Properties of Cycloparaffins Used to Model the Condensable Primary Organic Emissions.						
Compound	MW (g/mol)	p_L^o @ 298 K (atm)	Mass Fraction of CPEs	Concentration at High Toluene Concentration ^{1,4} ($\mu\text{g}/\text{m}^3$)	Concentration at Base Toluene Concentration ^{2,4} ($\mu\text{g}/\text{m}^3$)	Concentration at Low Toluene Concentration ^{3,4} ($\mu\text{g}/\text{m}^3$)
C ₁₈ H ₃₀	246	5.3E-09	0.20	16.4	8.2	4.1
C ₂₂ H ₃₆	300	1.6E-11	0.30	24.6	12.3	6.1
C ₂₆ H ₄₂	354	4.6E-14	0.17	13.7	6.9	3.4
C ₂₉ H ₄₆	390	1.7E-16	0.25	21.2	10.6	5.3
C ₃₇ H ₅₆	500	1.3E-23	0.08	6.4	3.2	1.6
Total			1.00	82.3	41.2	20.5

¹High toluene concentration = 352.6 $\mu\text{g}/\text{m}^3$
²Base toluene concentration = 176.3 $\mu\text{g}/\text{m}^3$
³Low toluene concentraion = 88.15 $\mu\text{g}/\text{m}^3$
⁴Total mass of condensable primary emissions scales as 23 $\mu\text{g}/\text{m}^3$ per 100 $\mu\text{g}/\text{m}^3$ of toluene

3.2. Task 2: Simulations

3.2.1. Base & Sensitivity Cases

While in principle would be possible to conduct baseline simulations and sensitivity analyses of aerosol formation for all six airsheds, it would not be possible to conduct all such model runs in a reasonable amount of time. Therefore, a “base case” set of VOC, oxidant, and NO_x concentrations was developed to be representative of VOC concentrations found in all six regions.

Observations discussed by Pankow *et al.* (2003), Tanaka *et al.* (2000), Derwent *et al.* (1998), Aneja *et al.* (1996), and Goldan *et al.* (1995), and state environmental website data were used to estimate reference concentrations (expressed as part-per-million mixing ratios) for the VOCs, oxidant (O₃), and NO_x (NO+ NO₂) within the ambient air of the six prototype areas discussed above. For the VOCs, the **reference** concentration for a particular VOC was taken to be the midpoint of the range of the median concentrations in the six airsheds. Median VOC concentrations in an airshed were calculated by spatially averaging available VOC measurements taken in that airshed. Individual VOC measurements were typically reported as a time average where the averaging interval ranged from 1 to 24 hours, depending on sampling location. As suggested above, to obtain the actual **base case** VOC conditions, the reference mixing ratios of each of the 10 study VOCs was then **boosted** so that the total mixing ratio of carbon for a specific type of compound (*e.g.*, aliphatic *n*-alkanes) was equivalent to that for the group of similar compounds among the group of 35. In this way, the base case mixing ratios of the 10 VOCs represent lumped parameterizations for an average atmosphere containing the 35 compounds.

The oxidant and NO_x base case concentrations were derived in a manner similar to that used for the VOCs except that: 1) that averaging times for the concentration measurements ranged from hourly to yearly (the majority were yearly); and 2) no concentration boosting was

carried out. The base case atmospheric temperature was set at 298 K, atmospheric pressure was assumed to be 1 atm, and the relative humidity was set at 68% for each run, these values being fairly typical of the meteorological conditions of the airsheds where the VOC concentrations were measured. Eight sensitivity cases were then developed based on the base case described above; these are summarized in Table 3. In the model, the initial concentration of propene was selected based on the concentrations of the ten primary VOCs.

Table 3. Initial Mixing Ratios (ppbV) for the Base Case Plus Eight Sensitivity Cases for the Ten Study VOCs. (Values Given Are After Boosting to Represent the Broader Mix of 35 Compounds.) Oxidant Concentrations are also Given. The Concentration Factor for a “High” Case is 2x Relative to the Base Case; the Concentration Factor for a “Low” Case is 0.5x Relative to the Base Case.

	<u>Case 1.</u>	<u>Case 2.</u>	<u>Case 3.</u>	<u>Case 4.</u>	<u>Case 5.</u>	<u>Case 6.</u>	<u>Case 7.</u>	<u>Case 8.</u>	<u>Case 9.</u>
anth. VOCs->	Base	High	Low	High	High	Low	Low	High	Low
biog VOCs->	Base	High	Low	High	High	Low	Low	Low	High
oxidants->	Base	Base	Base	High	Low	High	Low	Base	Base
constituent									
<u>anthropogenic VOCs</u>									
<i>n</i> -decane	135.9	271.7	67.9	271.7	271.7	67.9	67.9	271.7	67.9
2-methylhexane	50.6	101.2	25.3	101.2	101.2	25.3	25.3	101.2	25.3
toluene	47.7	95.4	23.8	95.4	95.4	23.8	23.8	95.4	23.8
1,2,4-trimethylbenzene	43.2	86.3	21.6	86.3	86.3	21.6	21.6	86.3	21.6
naphthalene	11.5	23.0	5.8	23.0	23.0	5.8	5.8	23.0	5.8
cyclohexane	9.9	19.9	5.0	19.9	19.9	5.0	5.0	19.9	5.0
<i>m</i> -xylene	15.5	30.9	7.7	30.9	30.9	7.7	7.7	30.9	7.7
<i>m</i> -ethyltoluene	15.1	30.3	7.6	30.3	30.3	7.6	7.6	30.3	7.6
4-methyl-1-pentene	4.0	8.1	2.0	8.1	8.1	2.0	2.0	8.1	2.0
<u>biogenic VOC</u>									
α -pinene	22.5	45.1	11.3	45.1	45.1	11.3	11.3	11.3	45.1
<u>oxidants</u>									
NO	285.1	285.1	285.1	570.2	142.6	570.2	142.6	285.1	285.1
NO ₂	110.0	110.0	110.0	220.0	55.0	220.0	55.0	110.0	110.0
O ₃	75.7	75.7	75.7	151.3	37.8	151.3	37.8	75.7	75.7

Within each of the total of nine cases in Table 3, four compounds were chosen for two sensitivity runs that would allow example determinations of the corresponding differential OPM formation potentials. These compounds were 2-methylhexane, α -pinene, toluene, and naphthalene. In the first sensitivity run, the individual initial mixing ratio was multiplied by 0.5x while holding all other initial mixing ratios constant. In the second sensitivity run, the individual initial mixing ratio was multiplied by 2x while holding all other initial mixing ratios constant.

3.2.2. Model Components of OPMBOX

3.2.2.1. The Chemical Kinetics Model

3.2.2.1.1. Description

The gas-phase chemistry model used in the current work to simulate formation of semi-volatile oxidation products capable of partitioning to the particle phase was developed in the same way as the Caltech Atmospheric Chemistry Mechanism (CACM). CACM has two main features: 1) state-of-the-art treatment of O₃ formation chemistry; and 2) explicit prediction of the time-dependent concentrations of second and third stage organic oxidation reaction products that can then condense to form OPM (Griffin *et al.*, 2002).

The CACM model uses surrogate structures to represent lumped chemical classes of VOCs, and that is the approach used here. Also, the basic chemical assumptions made in the development of CACM are used here while tracking the individual oxidation products of each of the ten identified parent compounds. These assumptions are based on the protocol for mechanism development published by Jenkin *et al.* (1997). To reduce computational demand, the current chemical model lumps secondary products (stable and radical) of similar carbon number and functionality while maintaining a carbon balance. In all, approximately 1200 reactions are needed to describe the oxidation of the ten VOCs and propene to the final product, carbon dioxide.

As an example, the assumed gas-phase chemistry of *n*-decane is shown in Figure 2. The oxidation of *n*-decane is assumed to proceed via only one pathway (H-atom abstraction in the 5-location). A whole suite of reactions is possible after initial oxidation occurs. Similar chemistry maps were made for each of the other nine VOC compounds, and for propene. Inorganic reactions involving NO_x, O₃, and other species such as nitric acid are also considered. Appropriate rate constants for the resulting 1202 reactions were based on: 1) published experimental data; 2) analogy with published experimental data; or 3) use of structure-reactivity relationships (Atkinson, 1990, 1994, 1997; Bierbach *et al.*, 1994; Goumri *et al.*, 1992; Kwok and Atkinson, 1995; Jenkin *et al.*, 1997; Stockwell *et al.*, 1997; Seinfeld and Pandis, 1998; Carter, 1999; Finlayson-Pitts and Pitts, 1999). In cases where stoichiometric reaction coefficients were not unity, yields were determined based on: 1) published experimental observations; 2) parameterizations (especially in the case of alkyl nitrate formation *vs.* NO to NO₂ conversion in peroxy radical reactions with NO); or 3) estimates based on chemical intuition (Carter and Atkinson, 1989; Atkinson, 1990, 1994, 1997; Jenkin *et al.*, 1997; Seinfeld and Pandis, 1998; Finlayson-Pitts and Pitts, 1999).

The above information was used in development of the computer code that describes concentrations of 478 species (both stable and radical) as a function of time. As a first step, the equations describing the reaction rate kinetic coefficients and appropriate stoichiometric coefficients as a function of temperature were coded. Next, equations to calculate radical species assumed to hold to the pseudo steady state assumption (PSSA) were implemented. These radical species concentrations are functions of either: 1) the concentrations of species that are available from the previous model time step; or 2) PSSA species calculated in the current model time step based on kinetic rate constants and stoichiometric yields. Code describing the forward rates of each of the 1202 reactions was then implemented. Based on these, for each integrated species,

expressions describing the rate of formation (A_i) and the rate of consumption divided by the species concentration (B_i) were implemented. This information is passed in the model to an existing integrator that numerically solves the differential equation $dC_i/dt = A_i - B_i C_i$ for C_i , the concentration of the species i , at each model time step.

The completed code was debugged and checked twice for any typographical errors. When it was certain that the code was correct, numerous test runs with highly unrealistic concentrations and conditions were performed to confirm that there would be consistent success in the convergence of the integrator solving the gas-phase kinetic expressions. In over 100 test cases, convergence was always achieved. Under these conditions, the gas-phase chemistry model simulates 600 minutes of model time in under 3 seconds real time.

Figure 3 provides example results for a trial case in which all VOC concentrations are initialized at 104 ppbv, the initial hydrocarbon to NO_x ratio = 5 ppmC/ppm, the NO to NO_2 ratio = 2, $T = 298.15$ K, and the relative humidity = 65%. With respect to rate of decay, species with lower kinetic rate constants for oxidation by the hydroxyl radical have the lowest rate of consumption. This indicates that the gas-phase chemistry is behaving appropriately. In addition, the simulations of formaldehyde oxidation in the formaldehyde- NO_x - O_3 system considered by Seinfeld (1986) were matched well by our model. Further confirmation of the behavior of the gas-phase kinetic model was achieved by examining the NO_x and O_3 behavior of a run in which base case NO_x and O_3 initial mixing ratios are used with unscaled mixing ratios of the ten VOC compounds of interest. These results are exhibited in Figure 4. Though difficult to discern in Figure 4, NO, NO_2 , and O_3 quickly enter the photostationary state relation for this system. After a short time, oxidation of the VOC compounds leads to formation of peroxy radicals that convert NO to NO_2 , the photolysis of which is a key step in the production of O_3 . Qualitatively, this

figure is extremely similar to results observed in numerous smog chamber experiments (*e.g.*, Griffin *et al.*, 1999).

As a last step to confirm that the behavior of the gas-phase model was correct before attempting to link it to the OPM condensation, individual product mixing ratios were investigated for the unscaled base case. These results are shown in Figure 5, which indicates the behavior of three products, A3 (a C₁₀ hydroxy ketone from the oxidation of *n*-decane), Q2 (pinonic acid, a C₁₀ keto-acid from the oxidation of α -pinene), and V6 (a C₇ diunsaturated keto-aldehyde from the oxidation of toluene). First consider species A3. A3 is formed as shown in Figure 2 by abstraction of an H-atom of *n*-decane by OH followed by the following steps: rapid addition of oxygen to form a peroxy radical; conversion of the peroxy radical to an alkoxy radical by reaction with NO; isomerization of the alkoxy radical via a 1,5-H atom shift to form a hydroxy alkyl radical; addition of oxygen to form a hydroxy peroxy radical; conversion of the hydroxy peroxy radical to an hydroxy alkoxy radical via reaction with NO; and, conversion of the hydroxy alkoxy radical to a hydroxy ketone via reaction with the hydroperoxy radical.

As shown in Figure 3, *n*-decane is one of less reactive of the ten primary VOCs. The functionality associated with product A3 does not increase the reactivity; therefore, because of the high initial mixing ratio of *n*-decane, the formation of product A3 is greater than its consumption throughout the model simulation. The opposite behavior is observed for Q2 and V6, whose parent VOCs are much more reactive. These products initially increase rapidly because they are first-generation products of the O₃- α -pinene reaction and toluene-OH reaction, respectively. Because of the increase in parent VOC reactivity and because the parent mixing ratios are smaller compared to *n*-decane, the formation of products V6 and Q2 are overwhelmed by consumption after approximately 5 hours. The behavior of these three oxidation products matches intuitive expectations. The results presented in Figures 3-5 support the view that the

gas-phase chemical mechanisms developed here adequately describe the atmospheric chemistry of the ten VOC compounds of interest.

3.2.2.1.2. General Applicability

Numerous assumptions were utilized in the development of the gas-phase kinetic model. These included estimation of stoichiometric yields, limiting oxidations to one major initial pathway (as with *n*-decane in Figure 2), and the estimation of kinetic rate constants that are not available in the literature. While these assumptions are not expected to drastically affect the simulated mixing ratios of the parent VOCs, NO_x, or O₃, they could affect the mixing ratios of the secondary products, thereby influencing the rate of production of OPM. For the monoterpenes, there is the added problem that reaction pathways and kinetic rate constants are very structure specific (Griffin *et al.*, 1999). Thus, high-biogenic VOC cases that are characterized by high levels of, for example β-pinene instead of α-pinene, cannot be considered to be modeled reliably by the current model. The explicit consideration of the oxidation of multiple mono-terpenes can, nevertheless, be built into subsequent revisions of the model. Overall, it can be concluded that the kinetic model developed here should be appropriately updated as knowledge in this area evolves, including consideration of any appropriate implications of recent assertions by Jang *et al.* (2002) regarding “heterogeneous acid-catalyzed chemistry”.

3.2.2.2. The OPM Formation Model

Governing Equations. OPMBOX is a fixed volume model. The underlying mathematical formalism and computational procedure that can be used to calculate the amounts of the individual compounds in the OPM phase were originally described by Pankow (1994b), and discussed again by Pankow *et al.* (2001) and Seinfeld *et al.* (2001). Briefly, the method

solves the matrix equation representation of a multicomponent gas/particle distribution, where each partitioning compound satisfies its own version of the gas/particle distribution equation for absorptive partitioning (Pankow, 1994a):

$$K_{p,i} = \frac{c_p \text{ (ng/}\mu\text{g)}}{c_g \text{ (ng/m}^3\text{)}} = \frac{RT f_{om}}{10^6 \text{MW}_{om} \zeta_i p_{L,i}^o} \quad (3)$$

where:

$K_{p,i}$ = gas/particle partition coefficient of compound i ;

c_p (ng/ μ g) = concentration of compound i in the particle phase;

c_g (ng/m³) = concentration of compound i in the gas phase;

R = ideal gas constant;

T (K) = temperature;

f_{om} = weight fraction of the PM that comprises the absorbing PM phase (= 1 in many cases of interest);

MW_{om} (g/mol) = average molecular weight of the absorbing PM phase; and

ζ_i = activity coefficient of compound i in the absorbing PM phase.

The governing matrix equation relates the individual mass concentrations of the compounds in the aerosol phase, F_i (ng m⁻³), to the total concentrations, T_i (ng m⁻³), and has the form (Pankow, 1994b; Pankow *et al.*, 2001):

$$\begin{bmatrix} F_1 \\ F_2 \\ \cdot \\ F_n \end{bmatrix} = \frac{M_o 760RT}{10^6 MW_{om}} \times \begin{bmatrix} \frac{(\zeta_1 p_{L,1}^o)^{-1}}{1 + K_{p,om1} M_o} & 0 & \cdot & \cdot \\ 0 & \frac{(\zeta_2 p_{L,2}^o)^{-1}}{1 + K_{p,om2} M_o} & \cdot & \cdot \\ \cdot & \cdot & \cdot & \cdot \\ \cdot & \cdot & \cdot & \frac{(\zeta_n p_{L,n}^o)^{-1}}{1 + K_{p,omn} M_o} \end{bmatrix} \begin{bmatrix} T_1 \\ T_2 \\ \cdot \\ T_n \end{bmatrix} \quad (4)$$

For any vector $\hat{\mathbf{T}}$ of T_i values, and assuming a guess value of M_o , equation 4 can be solved iteratively to determine the corresponding solution for the vector $\hat{\mathbf{F}}$ of F_i values. In each iteration, the ζ_i values are needed, and can be estimated probably to well within a factor of two using the UNIFAC method of Hansen *et al.* (1991).

After solving equation 4, there is no restriction that the resulting F_i will sum to give the guess value of M_o . In other words, it is not necessarily true that the result will satisfy

$$\sum_i F_i = 1000 M_o (\text{guess}) \quad (5)$$

This allows nonlinear optimization techniques to be used to calculate the correct value of M_o .

Pankow *et al.* (2001) defined the quantity ε

$$\varepsilon = \left| \sum_{i=1}^n F_i - 1000 M_o (\text{guess}) \right| \quad (6)$$

as an optimization parameter, and the calculation model developed here utilized an optimization scheme that varied the guess value M_o in search of $\varepsilon = 0$. Note that equation 6 always admits the

trivial solution ($\hat{\mathbf{F}} = 0, M_o = 0$). It is important to note that when the optimization finds *only* this solution, it can be concluded that OPM aerosol will not form for the conditions of interest (the system is “undersaturated”).

Input T_i Values. At each timestep, the total concentrations of each of the 174 oxidation products predicted by the atmospheric chemistry model are passed to the OPM formation model. The OPM formation model then iteratively solves equation 4 to minimize ϵ . Optimization to find the value of M_o that minimizes ϵ is performed by the Netlib optimization FORTRAN routine FMIN.FOR.

Input Vapor Pressure (p_L^o) Values. Because OPMBOX assumes a constant temperature, there is no need to dynamically estimate vapor pressures for the products. Therefore, p_L^o values for all 174 products have been coded into the model as a look-up table over the temperature range of 263 K to 313 K. Vapor pressures were estimated using one of two methods, depending on the molecular structure of the compound. If the compound structure could be expressed in terms of the UNIFAC groups for alkanes, alkenes, aromatics, alcohols, carbonyls, carboxylic acids then the vapor pressure estimation technique of Asher *et al.* (2001) was used. For compounds not representable in terms of UNIFAC groups (*e.g.*, compounds containing nitro/nitrate functionality as in PANs), the chemical property calculator SPARC was used (Hilal *et al.*, 1994). (Asher *et al.* (2001) provide a discussion of the uncertainty of the UNIFAC and SPARC methods.)

OPM Formation Model Validation. The underlying numerical procedure and theoretical framework of the OPM formation model used in OPMBOX has been validated through the modeling studies of Pankow *et al.* (2001) and Seinfeld *et al.* (2001). The specific implementation used in OPMBOX was tested by comparing OPM mass concentrations predicted by OPMBOX with those predicted using the model of Pankow *et al.* (2001) with a simplified set

of the oxidation products resulting from the atmospheric chemistry model. (Coding all 174 products utilized in OPMBOX into the Pankow *et al.* (2001) model would have represented a duplication of coding done with OPMBOX, rather than an independent test of OPMBOX.) The 174 products were sorted in terms of their p_L° values into 10 bins, and at the conclusion of each 600 min trial run, the total mass concentration of all products in a particular p_L° bin was calculated. Table 4 gives the vapor pressure ranges of the ten bins. A surrogate compound with a p_L° value in the range in question and with a chemical structure that could be represented in terms of the standard UNIFAC basis set used in the model of Pankow *et al.* (2001) was then chosen to represent the total mass of all products in that bin. The M_o value formed by OPMBOX for the complete set of 174 products could then be compared to that formed by the Pankow *et al.* (2001) model for the simplified set.

Table 4. p_L° Bins and Surrogate Compounds Used to Validate OPMBOX by Comparison with Pankow <i>et al.</i> (2001) Model.		
p_L° Bin Range (atm)	Surrogate Compound	Actual p_L° (atm)
$p_L^\circ < 10^{-10}$	1-nitro-3,4-dihydroxy-napthalene	2.0×10^{-14}
$10^{-10} \leq p_L^\circ < 10^{-9}$	2-hydroxy-propanedioic acid	1.9×10^{-10}
$10^{-9} \leq p_L^\circ < 10^{-8}$	3,5,6-trioxo-heptanoic acid	5.3×10^{-9}
$10^{-8} \leq p_L^\circ < 10^{-7}$	pinic acid	5.3×10^{-8}
$10^{-7} \leq p_L^\circ < 10^{-6}$	2,6-dihydroxy-toluene	5.7×10^{-7}
$10^{-6} \leq p_L^\circ < 10^{-5}$	3,6-dioxo-decane	4.1×10^{-6}
$10^{-5} \leq p_L^\circ < 10^{-4}$	4-oxo-2-pentenoic acid	3.4×10^{-5}
$10^{-4} \leq p_L^\circ < 10^{-3}$	4-hydroxy-butanal	2.2×10^{-4}
$10^{-3} \leq p_L^\circ < 10^{-2}$	cyclohexanone	3.1×10^{-3}
$p_L^\circ \geq 10^{-2}$	2-oxo-3-butene	1.0×10^0

Four simulations were run with OPMBOX with the starting parent VOC concentrations listed in Table 5. The final product concentrations at the end of each 600-minute simulation were used to compute the total product masses in each of the ten p_L^o bins listed in Table 4. These masses were then entered into the Pankow *et al.* (2001) OPM formation model, along with the structures of the 10 surrogate species. Table 6 gives the aerosol mass concentrations predicted by OPMBOX along with those predicted by the Pankow *et al.* (2001) model. Given the extent of the assumptions required to utilize the Pankow *et al.* (2001) model in this test, the results are seen to compare favorably, and are viewed as indicating that the OPM formation model included in OPMBOX is functioning correctly.

Table 5. Parent VOC Concentrations for OPMBOX Comparison with the Pankow <i>et al.</i> (2001) Model.				
Parent VOC	Trial 1 (ppbv)	Trial 2 (ppbv)	Trial 3 (ppbv)	Trial 4 (ppbv)
<i>n</i> -decane	1.04	10.4	104	1104
2-methylhexane	0.39	3.9	39	339
toluene	0.23	2.3	23	223
1,2,4-trimethylbenzene	0.21	2.1	21	221
α -pinene	0.14	1.4	14	114
naphthalene	0.09	0.9	9	99
cyclohexane	0.08	0.8	8	88
<i>m</i> -xylene	0.08	0.8	8	88
<i>m</i> -ethyltoluene	0.07	0.7	7	77
4-methyl-1-pentene	0.03	0.3	3	33

Table 6. Comparison of OPM Mass Concentrations Predicted by OPMBOX and by the Pankow <i>et al.</i> (2001) OPM Model.		
Trial Number	M_o (OPMBOX) $\mu\text{g}/\text{m}^3$	M_o (Pankow <i>et al.</i>) $\mu\text{g}/\text{m}^3$
1	0.013	0
2	5.7	1.4
3	54.5	26.6
4	1390	1427

3.3. Task 3. OPM Formation Results for Illustrative Conditions of Interest

3.3.1. OPM Formation in the Absence of Condensable Primary Emissions

The physical and environmental conditions common to all of the model runs of OPMBOX are summarized in Table 7. The final total organic aerosol mass concentration M_o for each simulation is given in Table 8. Using the data in

Table 7. Physical and Environmental Conditions Common to all Simulations Run Using OPMBOX for this Study.		
Atmospheric temperature (K)	=	298
Atmospheric pressure (atm)	=	1.0
Relative humidity (ppmv)	=	20900.0
Start time (minutes)	=	0
End time (minutes)	=	600
Latitude (decimal degrees N)	=	34.058
Longitude (decimal degrees W)	=	118.25
Starting time (hours after midnight)	=	8.0
Date (month/day/year)	=	8/27/1987
Fraction of aerosol that is abs. phase	=	1.0

Table 8, it is possible to consider the relationship between relative reactivity of a compound and the effect of variations in its initial concentration on M_o , all other conditions remaining the same.

Table 8. Final OPM Mass Concentrations M_o ($\mu\text{g}/\text{m}^3$) Predicted by OPMBOX for the VOC Sensitivity Simulations Run for this Study. M_o Values Given for Each Case, and for Each Case After Changing a Single VOC by a Factor of 0.5x (Low) and by a Factor of 2x (High).									
Case	M_o ($\mu\text{g}/\text{m}^3$)	Low 2-methyl hexane	High 2-methyl hexane	Low α -pinene	High α -pinene	Low toluene	High toluene	Low Napth.	High Napth.
		M_o ($\mu\text{g}/\text{m}^3$)							
1. Base	312	248	453	316	607	297	489	312	524
2. Low VOC-Base Ox	20.2	16.3	30.8	16.8	36.0	14.0	30.9	20.2	40.0
3. High VOC-Base Ox	1360	1220	1470	1220	1720	1270	1520	1360	1640
4. High VOC-High Ox	915	704	1220	872	1580	869	1300	915	1300
5. High VOC-Low Ox	947	877	971	929	1094	883	1005	947	1090
6. Low VOC-High Ox	0.240	0.221	0.287	0.244	0.522	0.247	0.280	0.240	0.443
7. Low VOC-Low Ox	87.1	74.3	127	83.3	167	66.4	139	87.1	172
8. Low Anth-High Bio	209	103	252	207	629	191	260	209	338
9. High Anth-Low Bio	1080	1080	1210	1050	1210	917	1260	1080	1380

Figures 6-14 give M_o vs. VOC_{init} , which is the initial concentration of the parent VOC that is being varied for each of the nine cases. Table 9 provides the θ_{OPM} slopes obtained from linear regressions of these results. Although the slope of the line for any particular compound is case dependent (*e.g.*, the slope for naphthalene in Case 1 is not the same as in any other of the cases, there are several clear trends observable in the data which are discussed briefly below.

Table 9. θ_{OPM} Values ($\partial M_o / \partial VOC_{init}$; units: $\mu\text{g}/\text{m}^3$ per $\mu\text{g}/\text{m}^3$) in the Nine Cases (see Figures 6-14).				
Case	naphthalene	α -pinene	toluene	2-methyl hexane
1. Base	2.56	1.94	0.656	0.452
2. Low VOC-Base Ox	0.583	0.214	0.104	0.0704
3. High VOC-Base Ox	2.05	1.34	0.364	0.166
4. High VOC-High Ox	2.44	2.36	0.801	0.509
5. High VOC-Low Ox	1.16	0.583	0.148	0.0385
6. Low VOC-High Ox	0.00468	0.00341	0.000270	0.000310
7. Low VOC-Low Ox	2.37	1.00	0.414	0.256
8. Low Anth-High Bio	3.36	1.45	0.391	0.275
9. High Anth-Low Bio	3.00	2.54	0.359	0.193

The term Relative Incremental Aerosol Reactivities has been introduced in the literature relative to the issue of ozone formation potentials (Griffin *et al.*, 1999b). By analogy, Figure 15 therefore provides a plot of θ ratios for naphthalene to α -pinene, naphthalene to toluene, and naphthalene to 2-methylhexane, all vs. M_o . (The corresponding values are given in Table 10.) Since all of the plotted θ ratios are larger than unity, Figure 15 illustrates that θ for naphthalene is larger than θ for the other compounds for all of the cases considered. This is undoubtedly due in part to the high reactivity of naphthalene with atmospheric oxidants. We also conclude that for all the cases considered, $\theta_{\alpha\text{-pinene}}$ is greater than θ_{toluene} , and that θ_{toluene} is greater than $\theta_{\text{2-methyl hexane}}$.

Table 10. θ_i/θ_j Ratios (Relative Differential OPM Formation Potentials) for Selected Compounds in Nine Cases (see Figure 15.)			
Case	$\frac{\theta_{\text{naphthalen e}}}{\theta_{\alpha\text{-pinene}}}$	$\frac{\theta_{\text{naphthalen e}}}{\theta_{\text{toluene}}}$	$\frac{\theta_{\text{naphthalen e}}}{\theta_{\text{2-methyl hex}}}$
1. Base	1.3	3.9	5.7
2. Low VOC-Base Ox	2.7	5.6	8.3
3. High VOC-Base Ox	1.5	5.6	12
4. High VOC-High Ox	1.0	3.0	4.8
5. High VOC-Low Ox	2.0	7.9	30
6. Low VOC-High Ox	1.4	17	15
7. Low VOC-Low Ox	2.4	5.7	9.2
8. Low Anth-High Bio	2.3	8.6	12
9. High Anth-Low Bio	1.2	8.4	16

Figure 16 provides a time series plot of the concentrations of NO, NO₂, and O₃ for the entire 600-minute simulation of the Low VOC-High Ox case (Case 6), and for the Low VOC-Low Ox case (Case 7). When the initial NO and NO₂ concentrations are low, NO is destroyed rapidly, leading to a maximum in the NO₂ concentration, and increasing O₃ levels. This decreased O₃ level for the high-oxidant cases relative to the low-oxidant cases leads to reduced levels of SOA and smaller values for M_0 .

Figure 17 shows the dependence in M_0 vs. the initial VOC_{TOTAL}, at different levels of initial oxidant. OPMBOX tracks the concentrations of all 174 products, along with the concentrations of the atmospheric oxidants, NO_x, CO, and CO₂. As an example of the detail

available, the model output can be used to investigate mass fraction of carbon reacted that is converted into CO₂.

Figure 18 shows the total mass of carbon reacted as a function of reaction time and the total mass of carbon produced as CO₂ as a function of time for the base case scenario. Also plotted in Figure 18 is the fraction of carbon produced as CO₂. This shows that at the end of the 10-hour model run for Figure 18, roughly 5% of the total carbon reacted has been converted to CO₂. This result is typical of all nine cases listed in Table 3, with the conversion of reacted carbon mass to CO₂ consistently being approximately 5%.

It is obviously not possible for this report to investigate the dependence of OPM formation potentials on all conditions of interest for each parent VOC. Interested researchers can use OPMBOX for particular cases of interest not considered here.

3.3.2. Task 3.2: Effect of Condensable Primary Emissions on Aerosol Mass

The effect of CPEs on the formation of M_o was examined for three cases. These were the Low VOC-Base Oxidant, Base VOC-Base Oxidant, and High VOC-Base Oxidant cases. In each instance, the final values of all product concentrations were sorted according to vapor pressure into the ranges defined in Table 4. The total product mass in a particular vapor pressure range was calculated and then that mass was assumed to be completely due to the surrogate compound listed in Table 4. The product masses for each case were then used along with the corresponding CPE levels in Table 2. In general, the CPEs have a larger relative effect at low M_o levels.

Table 11. M_o Predicted using the Pankow <i>et al.</i> (2001) OPM Formation Model in the Absence and Presence of CPEs.			
Case	M_o (No Condensables) ($\mu\text{g}/\text{m}^3$)	M_o (Condensables) ($\mu\text{g}/\text{m}^3$)	Ratio
LowVOC-BaseOx	39.7	45.1	1.14
BaseVOC-BaseOx	456	486	1.07
HighVOC-BaseOx	1540	1600	1.04

3.4 Task 4. Implications of the Study for Laboratory Chamber Experiments

The preceding sections of this report describe an approach for predicting OPM formation potential (θ) values of particular VOCs under variable conditions. The corresponding predictions that have been made are based on a state-of-the-art gas-phase chemical mechanism coupled with and a gas-particle partitioning model. Evaluation of predicted OPM formation potentials against those measured experimentally in laboratory chambers will provide important information on the extent to which our current theoretical understanding reflects the behavior of actual systems.

OPM formation may result not only from condensation of first-generation oxidation products, but also from that of second- and higher-generation oxidation products. For example, based on chamber data, it has been suggested that OPM formation from toluene oxidation initiated by OH attack actually results from condensation of products of OH, NO_3 , or O_3 oxidation of first-generation OH oxidation products (Hurley *et al.*, 2001). This inference was based on the character of the OPM concentration *vs.* time data. Comparison of observed and predicted concentration *vs.* time curves will allow assessment of the fidelity of the theoretical chemical mechanisms as well as of the overall prediction of OPM formation amounts. Parent VOCs important in OPM formation can be categorized into the following classes:

- aromatics
- alkanes
- alkenes, both acyclic and cyclic
- biogenics

Table 1 lists the parent VOCs considered in this study, based on their prevalence in urban and regional atmospheres.

Most previous chamber studies have been designed to measure the fractional mass yield, Y . Based on existing chamber data (see Seinfeld and Pankow (2003) for a summary), aromatic and biogenic VOCs exhibit the largest fractional mass yields among compounds that have been studied. The current study confirms that these two classes of compounds merit continued study. Alkenes (and especially cyclic alkenes), which can lead to OPM by reaction with both OH and O_3 reactions, are also an important OPM-forming species. Therefore, on the basis of overall atmospheric importance to OPM formation, further chamber studies of aromatics, biogenics, and cyclic alkenes are recommended.

We also recommend that an overlapping systematic study of multiple VOCs within important compound classes be evaluated for the extent to which parent-dependent differences in OPM formation potential can be observed experimentally, as well as predicted by chemical mechanism and gas-particle partitioning modeling. The cyclic alkenes represent an ideal set of compounds in this regard. The number of carbon atoms, location of the double bond, and existence of side groups on the basic ring can be varied.

In summary, we recommend for the first category of studies that the following parent VOCs be studied experimentally in chamber experiments:

- toluene
- 1,2,4 – trimethylbenzene
- α - pinene
- naphthalene

In the second category of studies, a series of cyclic alkenes would be evaluated for their OPM formation potentials. Both O₃ dark oxidation and photochemical NO_x oxidation (both OH and O₃ reactions) should be carried out. The VOCs recommended for study are:

- cyclopentene
- cyclohexene
- cycloheptene
- 1-methyl cyclopentene
- 1-methyl cyclohexene
- 1-methyl cycloheptene
- methylene cyclohexane

4. References

- Aneja, V.P., Kim, D.S., Das, M., Hartsell, B.E. (1996) Measurements and analysis of reactive nitrogen species in the rural troposphere of southeast United States: Southern oxidant study site SONIA. *Atmos. Environ.*, **30** 649-659.
- Asher, W.E., Erdakos, G.B., Seinfeld, J.H., Pankow, J.F. (2001) Estimating the vapor pressures of multi-functional oxygen-containing organic compounds using group contribution methods. *Atmos. Env.*, **36**, 1483-1498.
- Atkinson, R. (1990) Gas-phase tropospheric chemistry of organic compounds: a review, *Atmos. Env.*, **24A**, 1-41.
- Atkinson, R. (1994) Gas-phase tropospheric chemistry of organic compounds, *J. Phys. Chem Ref. Data, Monograph 2*, 1-216.
- Atkinson, R. (1997) Gas-phase tropospheric chemistry of volatile organic compounds: 1. Alkanes and alkenes, *J. Phys. Chem. Ref. Data*, **26**, 215-290.
- Bierbach, A., Barnes, I., Becker, K.H., Wiesen, E. (1994) Atmospheric chemistry of unsaturated carbonyls: butenedial, 4-oxo-2-pentenal, 3-hexene-2,5-dione, maleic anhydride, 3H-furan-2-one, and 5-methyl-3H-furan-2-one, *Environ. Sci. Technol.*, **28**, 715-729.
- Carter, W.P.L., Atkinson, R. (1989) Alkyl nitrate formation from the atmospheric photooxidation of alkanes: a revised estimation method, *J. Atmos. Chem.*, **8**, 165-173.
- Carter, W.P.L. (1999) SAPRC-99, available via ftp (<http://helium.ucr.edu/~carter/>).
- Derwent, R.G., Jenkin, M.E., Saunders, S.M., Pilling, M.J. (1998) Photochemical ozone creation potentials for organic compounds in northwest Europe calculated with a master chemical mechanism. *Atmos. Env.*, **32**, 2429-2441.
- Finlayson-Pitts, B.J., Pitts, J.N. (1999) *Chemistry of the Upper and Lower Atmosphere*, Academic Press, New York.
- Fraser, M.P., G.R. Cass, B.R.T. Simoneit and R.A. Rasmussen (1997) Air quality model evaluation data for organics. 4. C₂-C₃₆ non aromatic hydrocarbons, 2356-2367.
- Goldan, P.D., Kuster, W.C., Fehsenfeld, F.C., Montzka, S.A. (1995) Hydrocarbon measurements in the southeastern United States: The Rural Oxidants in the Southern Environment (ROSE) program 1990. *J Geophys. Res.*, **100**, 25945-25963.
- Goumri, A., Elmaimouni, L., Sawyersyn, J.-P., Devolder, P. (1992) Reaction rates at (297 +/- 3) K of four benzyl-type radicals with O₂, NO, and NO₂ by discharge flow/laser induced fluorescence, *J. Phys. Chem.*, **96**, 5395-5400.
- Griffin, R.J., Cocker III, D.R., Flagan, R.C., Seinfeld, J.H. (1999a) Organic aerosol formation from the oxidation of biogenic hydrocarbons, *J. Geophys. Res.*, **104**, 3555-3567.
- Griffin, R. J. Cocker III, David R. Seinfeld, J.H. (1999b) Incremental aerosol reactivity: application to aromatic and biogenic hydrocarbons. *Env. Sci. Tech.* **33**, 2403-2408.
- Griffin, R.J., Dabdub, D., Seinfeld, J.H. (2002) Secondary organic aerosol: I. Atmospheric chemical mechanism for the production of molecular constituents, *J. Geophys. Res.*, **107**, 4332, doi:10.1029/2001JD000541.

- Hansen, H. K., Rasmussen, P., Fredenslund, A., Schiller, M., Gmehling, J. (1991) Vapor-liquid-equilibria by UNIFAC group contribution.5. Revision and extension, *Ind. Eng. Chem. Res.* **30**, 2352-2355.
- Harley, R.A., Hannigan, M.P., Cass, G.R. (1992) Respeciation of organic gas emissions and the detection of excess unburned gasoline in the atmosphere, *Env. Sci. Tech.* **26**, 2395-2408.
- Hurley, M.D., Sokolov, O., Wallington, T.J., Takekawa, H., Karasawa, M., Klotz, B., Barnes, I., Becker, K.H. (2001) Organic aerosol formation during the atmospheric degradation of toluene, *Env. Sci. Technol.*, **35**, 1358-1366.
- Hilal, S.H., Carreira, L.A. and Karickhoff, S.W. (1994) Estimation of chemical reactivity parameters and physical properties of organic molecules using SPARC. In: P.P.a.J.S. Murray (Editor), *Quantitative Treatments of Solute/Solvent Interactions*, Elsevier, Amsterdam.
- Jang, M.S., Czoschke, N.M., Lee, S., Kamens, R.M. (2002) Heterogeneous atmospheric aerosol production by acid-catalyzed particle-phase reactions, *Science*, **298**, 814-817.
- Jenkin, M.E., Saunders, S.M., Pilling, M.J. (1997) The tropospheric degradation of volatile organic compounds: a protocol for mechanism development, *Atmos. Environ.*, **31**, 81-104.
- Kwok, E.S.C., Atkinson, R. (1995) Estimation of hydroxyl radical reaction rate constants for gas-phase organic compounds using a structure-reactivity relationship: an update, *Atmos. Environ.*, **29**, 1685-1695.
- Odum, J.R., Hoffmann, T., Bowman, F., Collins, D., Flagan, R.C., Seinfeld, J. H. (1996) Gas/particle partitioning and secondary organic aerosol yields, *Env. Sci. Technol.*, **30**, 2580-2585.
- Pankow, J. F. (1994a) An absorption model of gas/particle partitioning of organic compounds in the atmosphere. *Atmos. Env.*, **28**, 185-188.
- Pankow, J.F. (1994b) An absorption model of the gas/aerosol partitioning involved in the formation of secondary organic aerosol. *Atmos. Env.*, **28**, 189-193.
- Pankow, J.F., Seinfeld, J.H., Asher, W.E., Erdakos, G.B. (2001) Modeling the formation of secondary organic aerosol. I. Application of theoretical principles to measurements obtained in the α -pinene/, β -pinene/, sabinene/, Δ^3 -carene/, and cyclohexene/ozone systems, *Env. Sci. Technol.* **35**: 1164-1172
- Pankow, J. F., Luo, W., Bender, D. A., Isabelle, L. M., Zogorski, J. S. (2003) Measurements of 87 Volatile Organic Compound (VOC) Contaminants in the Ambient Air of 13 Semi-Rural to Urban Locations in Maine, Massachusetts, New Jersey, Pennsylvania, Ohio, and Illinois, and California. Submitted to *Atmos. Environ.*
- Schauer, J.P., Fraser, M.P., Cass, G.R., and Simoneit, B.R.T. (2002) Source reconciliation of atmospheric gas-phase and particle-phase pollutants during a severe photochemical smog episode, *Env. Sci. Tech.* **36**, 3806-3814.
- Seinfeld, J.H. (1986) *Atmospheric Chemistry and Physics of Air Pollution*, Wiley-Interscience, New York.
- Seinfeld, J. H., Pandis, S.N., (1998). *Atmospheric Chemistry and Physics: From Air Pollution to Climate Change*, Wiley-Interscience, New York.

- Seinfeld, J.H., Asher, W.E., Erdakos, G.B., Pankow, J.F. (2001) Modeling the formation of secondary organic aerosol (SOA). 2. The predicted effects of relative humidity on aerosol formation in the α -pinene-, β -pinene-, sabinene-, Δ^3 -carene-, and cyclohexene-ozone systems. *Env. Sci. Technol.*, **35**, 1806-1817.
- Seinfeld, J.H., Pankow, J.F. (2003) Organic atmospheric particulate matter, *Annual Rev. Phys. Chem.*, **54**, 121-140.
- Stockwell, W.R., Kirchner, F., Kuhn, M., Seefeld, S. (1997) A new mechanism for regional atmospheric chemistry modeling, *J. Geophys. Res.*, **102**, 25,847-25,879.
- Tanaka, P.L., Oldfield S., Neece J.D., Mullins C.B., Allen D.T. (2000) Anthropogenic sources of chlorine and ozone formation in urban atmospheres. *Env. Sci. Technol.*, **34**, 4470-4473.

5. List of Figures

- Figure 1: The structures of the ten VOC compounds chosen for mechanistic study in this project.
- Figure 2: An example of the chemistry (for *n*-decane) determined using the mechanistic protocol of Jenkin *et al.* (1997).
- Figure 3: Gas-phase concentrations of the parent VOC's for the cases discussed in the text.
- Figure 4: NO_x-O₃ behavior in the unscaled base case discussed in the text.
- Figure 5: Behavior of specific gas-phase oxidation products in the unscaled base case discussed in the text.
- Figure 6: Base case (Case 1) sensitivity plots of the final organic aerosol mass M_O vs. one initial VOC concentration (slope = q).
- Figure 7: Low VOC-Base Ox (Case 2) sensitivity plots of the final organic aerosol mass M_O vs. one initial VOC concentration (slope = q).
- Figure 8: High VOC-Base Ox (Case 3) sensitivity plots of the final organic aerosol mass M_O vs. one initial VOC concentration (slope = q).
- Figure 9: High VOC-High Ox (Case 4) sensitivity plots of the final organic aerosol mass M_O vs. one initial VOC concentration (slope = q).
- Figure 10: High VOC-Low Ox (Case 5) sensitivity plots of the final organic aerosol mass M_O vs. one initial VOC concentration (slope = q).
- Figure 11: Low VOC-High Ox (Case 6) sensitivity plots of the final organic aerosol mass M_O vs. one initial VOC concentration (slope = q).
- Figure 12: Low VOC-Low Ox (Case 7) sensitivity plots of the final organic aerosol mass M_O vs. one initial VOC concentration (slope = q).
- Figure 13: Low Anth VOC- High Bio VOC - Base Ox (Case 8) sensitivity plots of the final organic aerosol mass M_O vs. one initial VOC concentration (slope = q).
- Figure 14: High Anth VOC- Low Bio VOC - Base Ox (Case 9) sensitivity plots of the final organic aerosol mass M_O vs. one initial VOC concentration (slope = q).
- Figure 15: Ratios for naphthalene to α -pinene, naphthalene to toluene, and naphthalene to 2-methyl hexane vs. M_O for the study cases.
- Figure 16: Plot of the time series of NO, NO₂, and O₃ concentrations calculated by OPMBOX for: a. Low VOC- High Oxidant Case (6) (top panel); and b. Low VOC – Low Oxidant Case (7) (bottom panel).
- Figure 17: Plot of the organic particulate mass concentration M_O calculated using OPMBOX as a function of total mass of initial parent VOC (VOC_{TOTAL}) for the three different initial Ox levels.
- Figure 18: Plot of time evolution of the total carbon mass reacted for the Base Case scenario plotted along with the carbon mass of CO₂ produced. Also shown is the fraction (in terms of per cent) of the total carbon mass reacted that has been converted to CO₂.

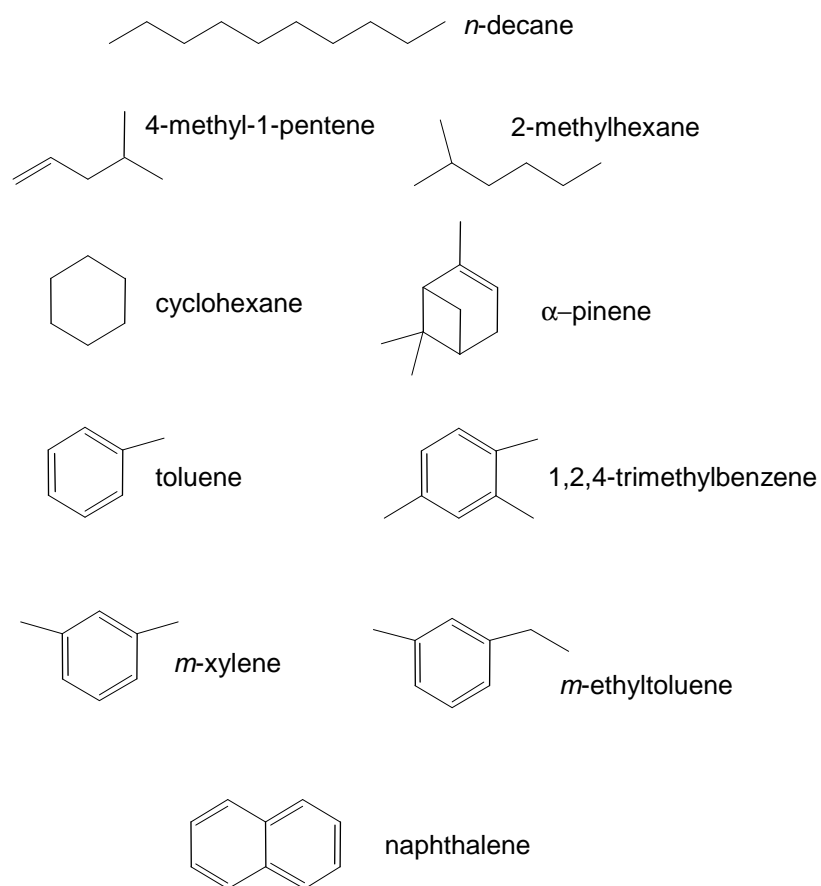


Figure 1. The structures of the ten VOC compounds chosen for mechanistic study in this project.

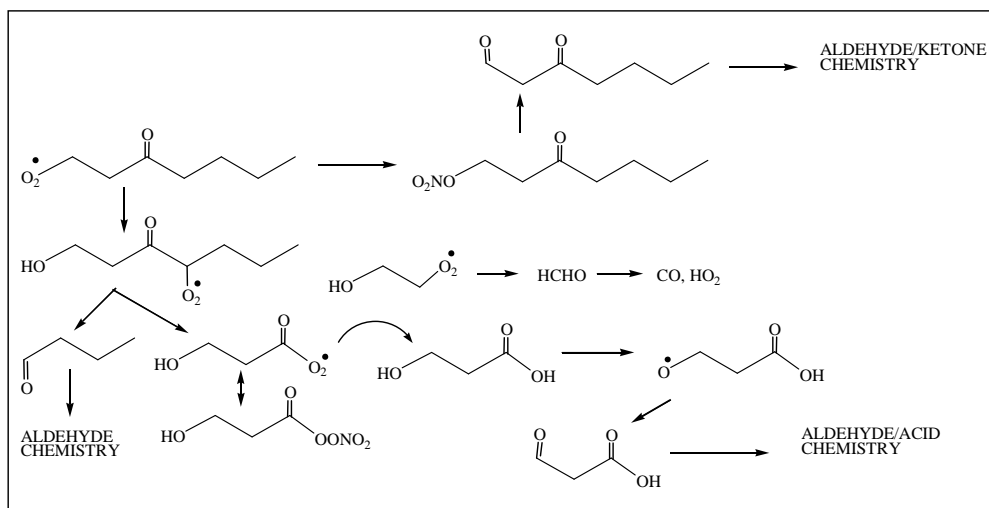
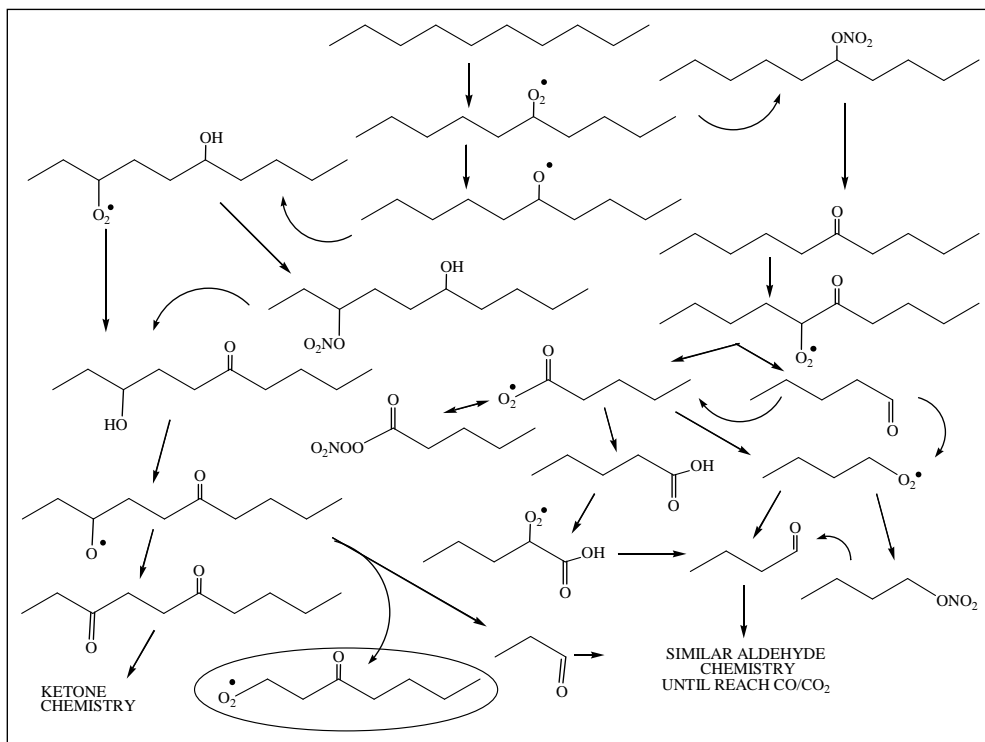


Figure 2. An example of the chemistry (for *n*-decane) determined using the mechanistic protocol of Jenkin *et al.* (1997).

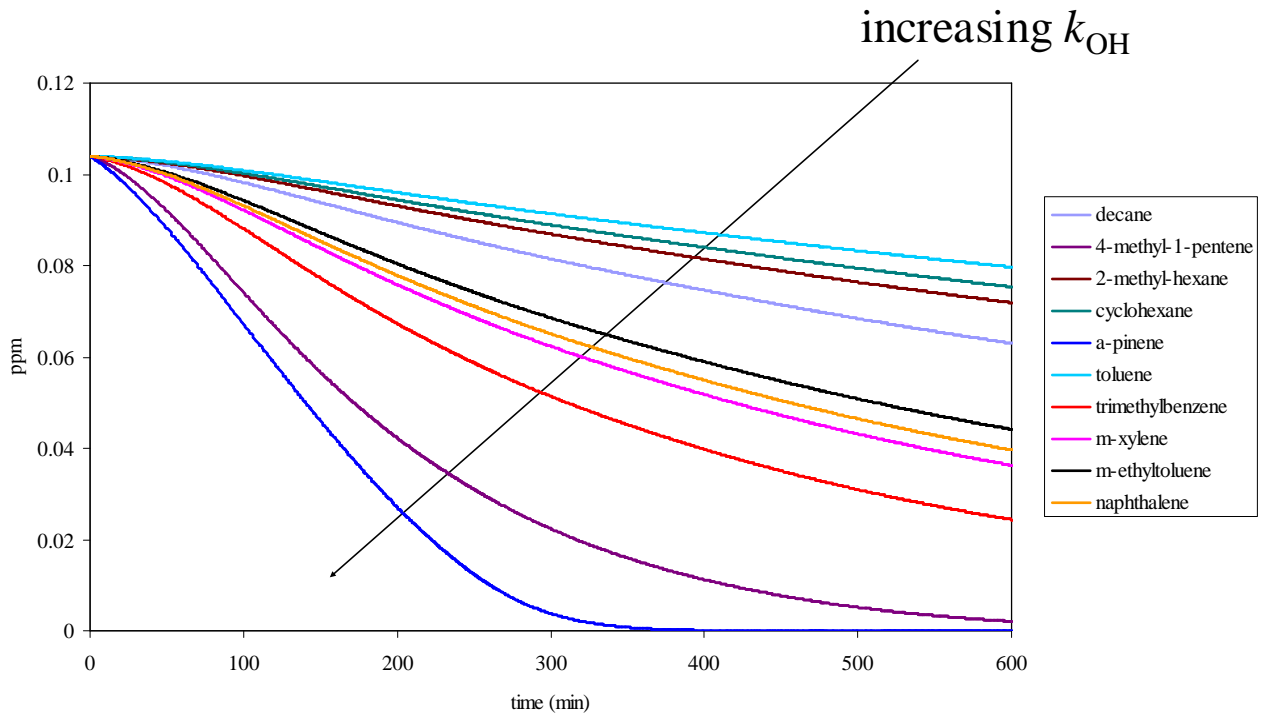


Figure 3. Gas-phase concentrations of parent VOC compounds in the case discussed in the text.

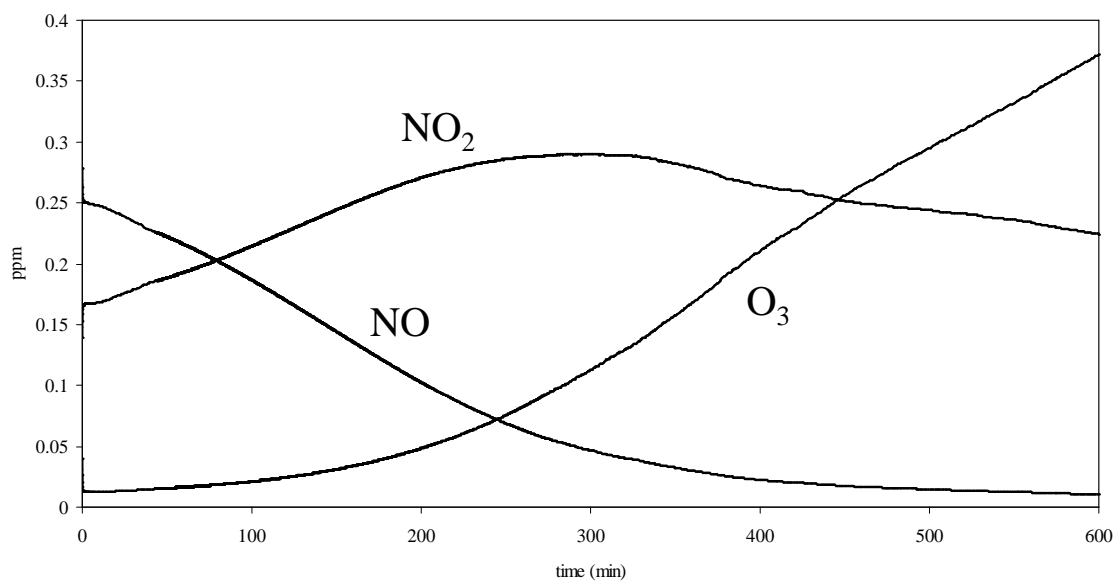


Figure 4. NO_x-O₃ behavior in the unscaled base case discussed in the text.

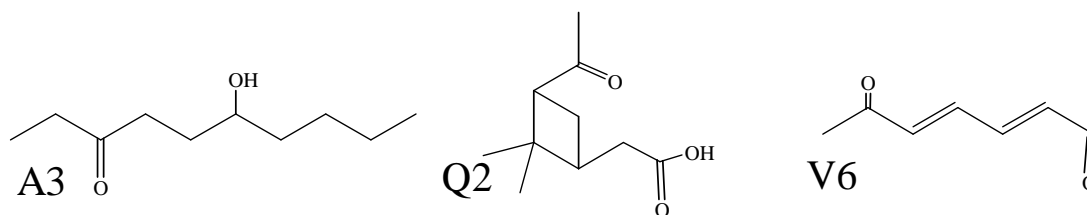
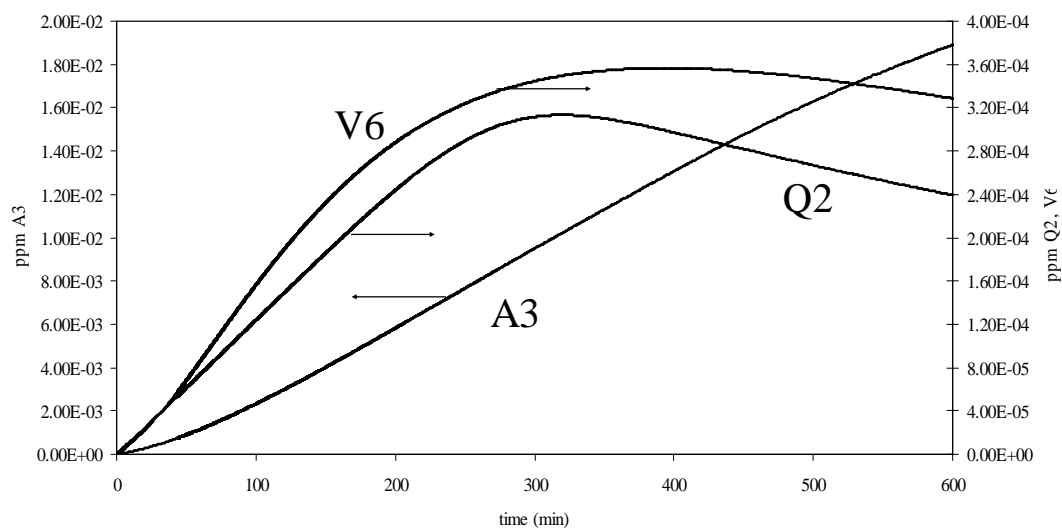


Figure 5. Behavior of specific gas-phase oxidation products in the unscaled base case discussed in the text.

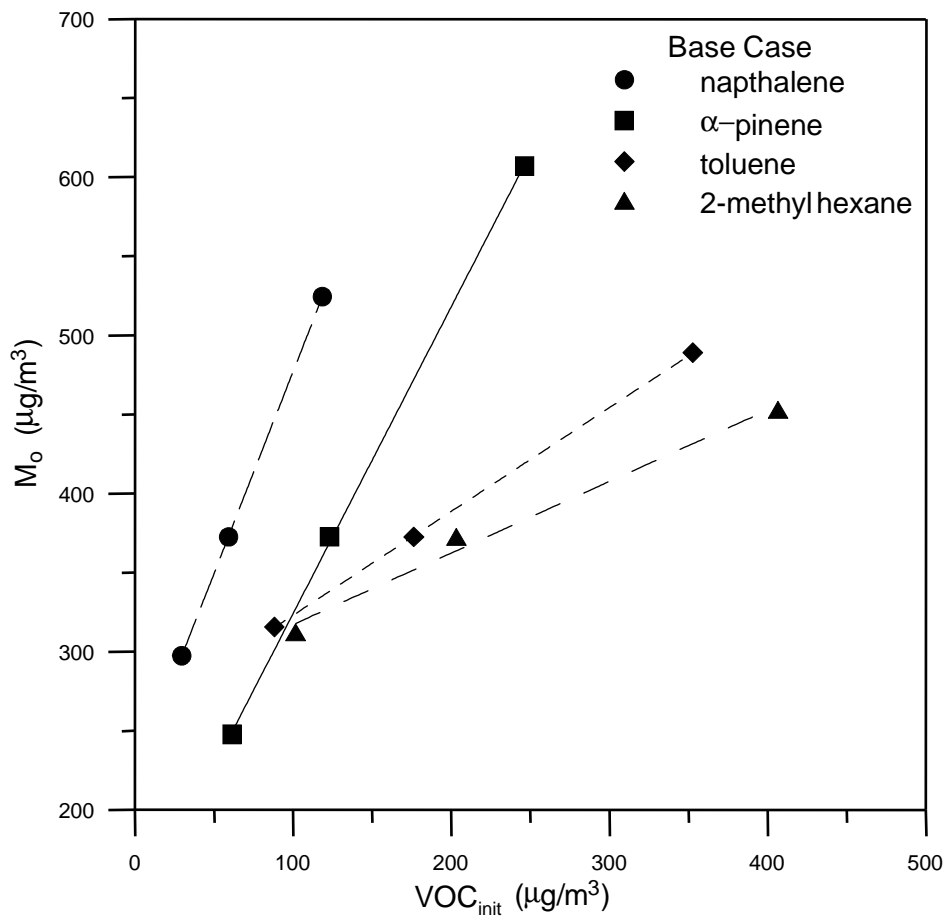


Figure 6. Base case (Case 1) sensitivity plots of the final organic aerosol mass M_o vs. one initial VOC concentration (slope = θ).

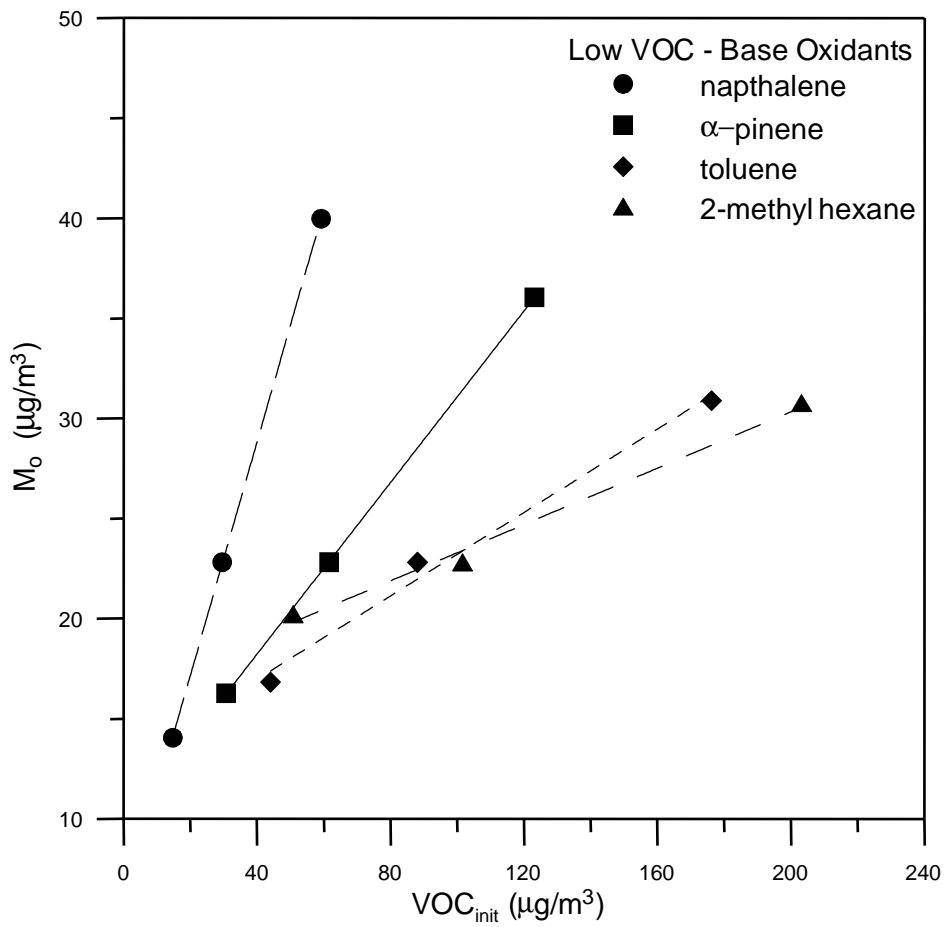


Figure 7. Low VOC-Base Ox (Case 2) sensitivity plots of the final organic aerosol mass M_o vs. one initial VOC concentration (slope = θ).

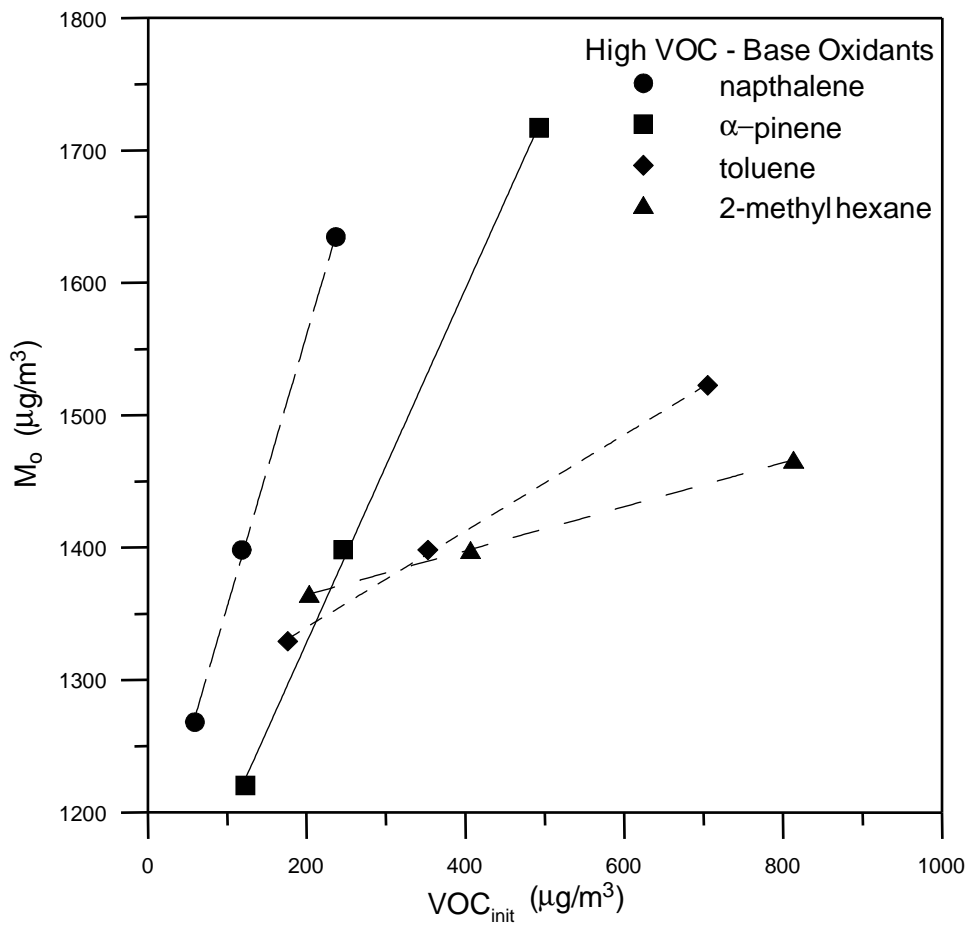


Figure 8. High VOC-Base Ox (Case 3) sensitivity plots of the final organic aerosol mass M_o vs. one initial VOC concentration (slope = θ).

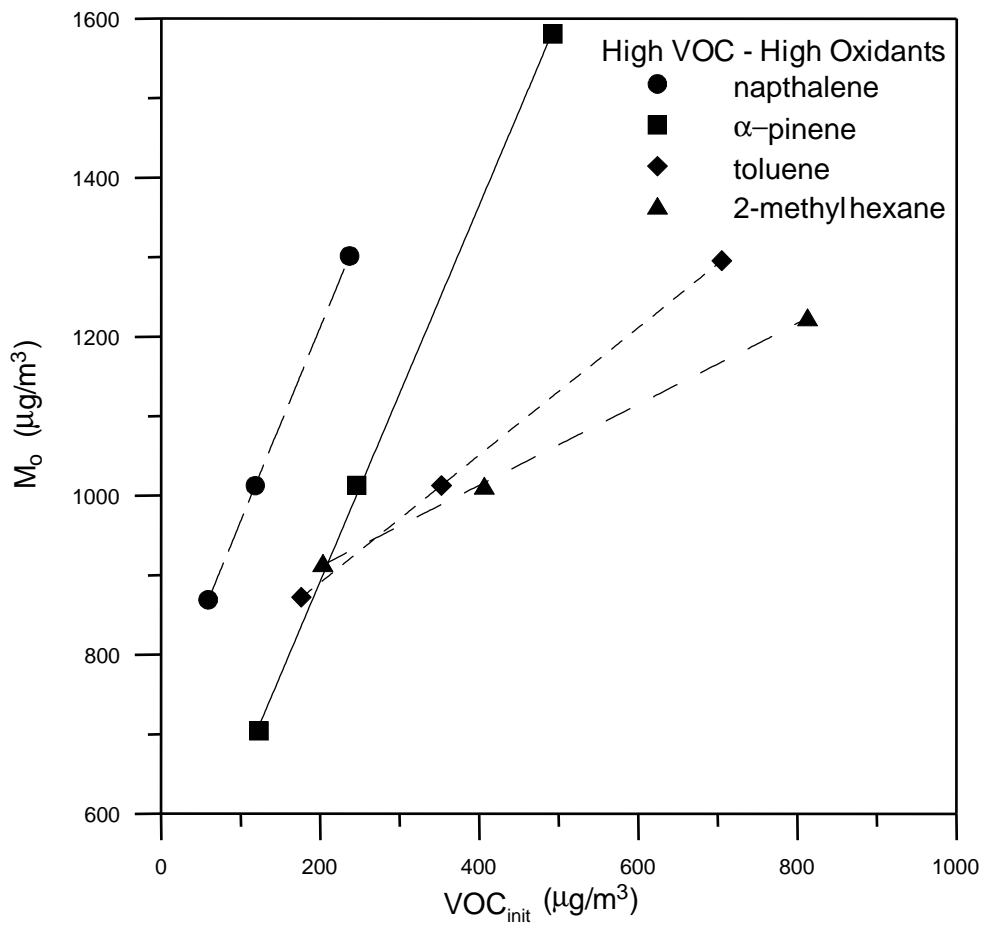


Figure 9. High VOC-High Ox (Case 4) sensitivity plots of the final organic aerosol mass M_o vs. one initial VOC concentration (slope = θ).

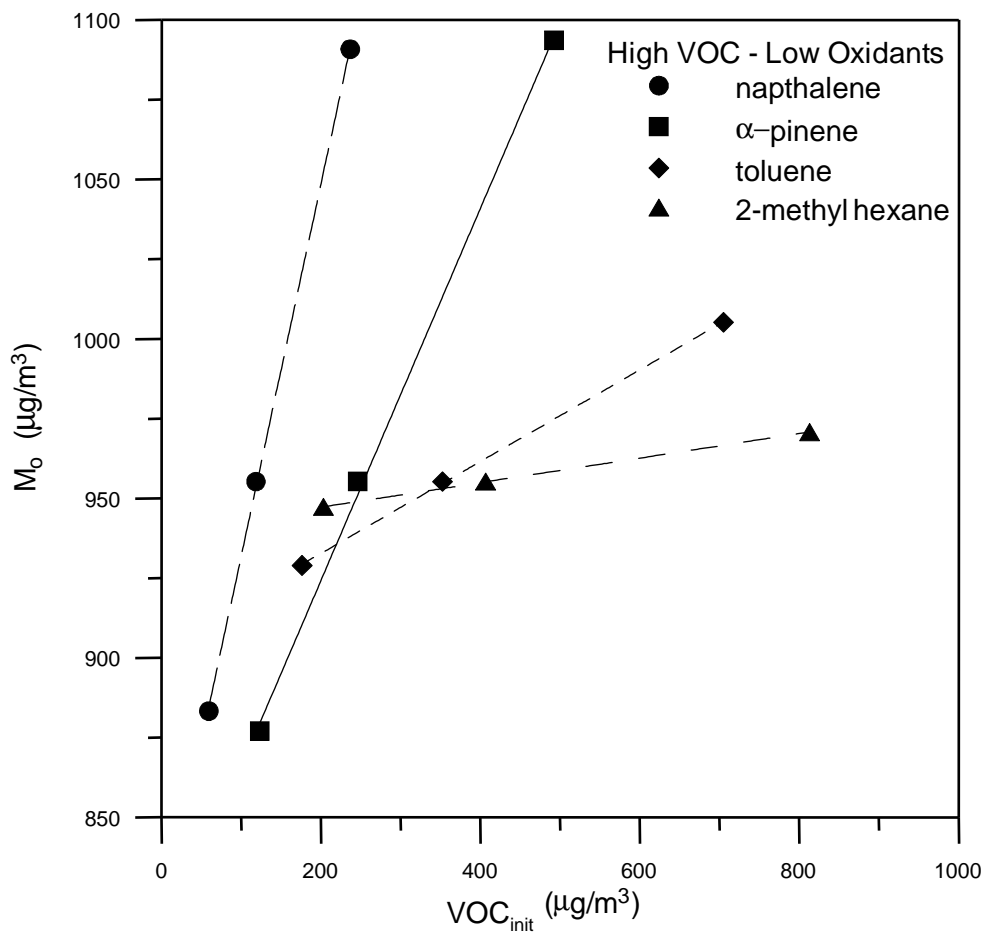


Figure 10. High VOC-Low Ox (Case 5) sensitivity plots of the final organic aerosol mass M_o vs. one initial VOC concentration (slope = θ).

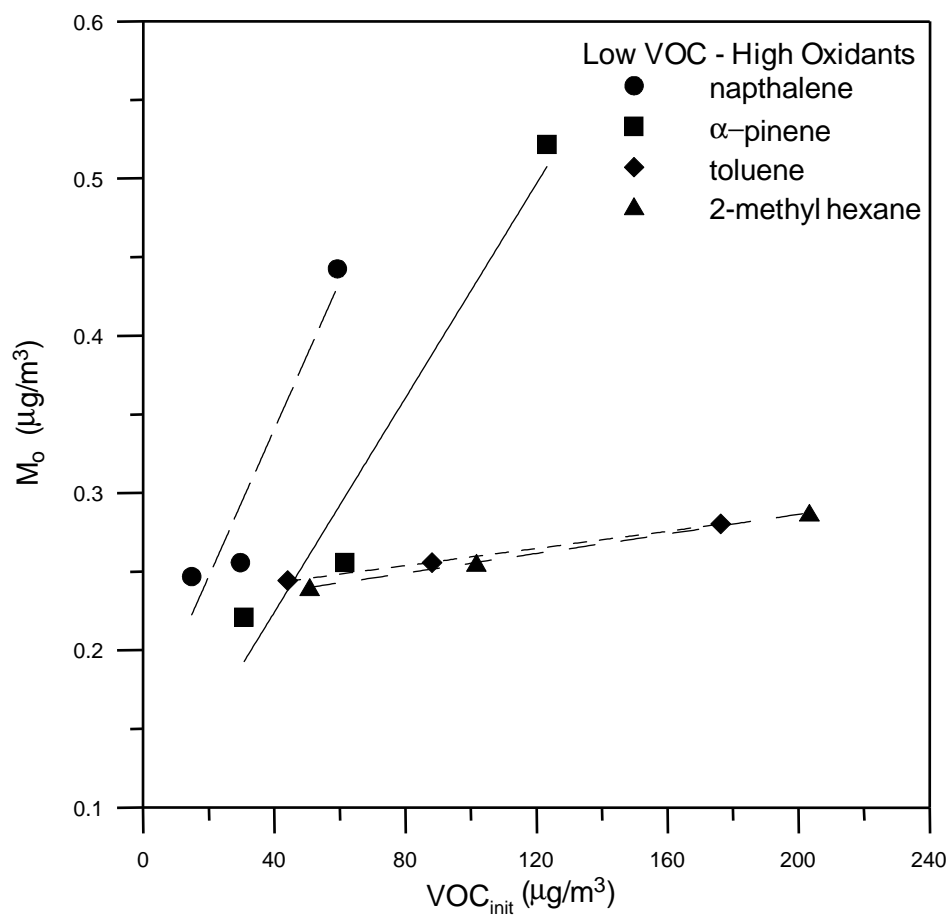


Figure 11. Low VOC-High Ox (Case 6) sensitivity plots of the final organic aerosol mass M_o vs. one initial VOC concentration (slope = θ).

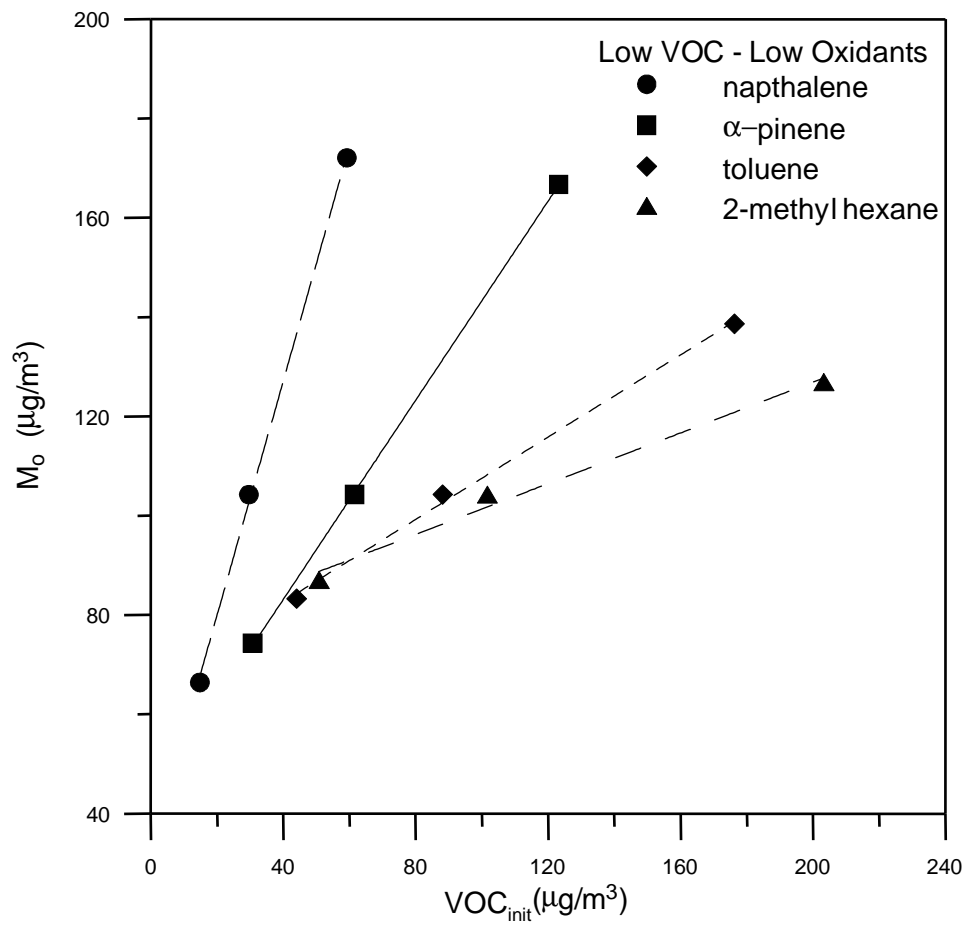


Figure 12. Low VOC-Low Ox (Case 7) sensitivity plots of the final organic aerosol mass M_o vs. one initial VOC concentration (slope = θ).

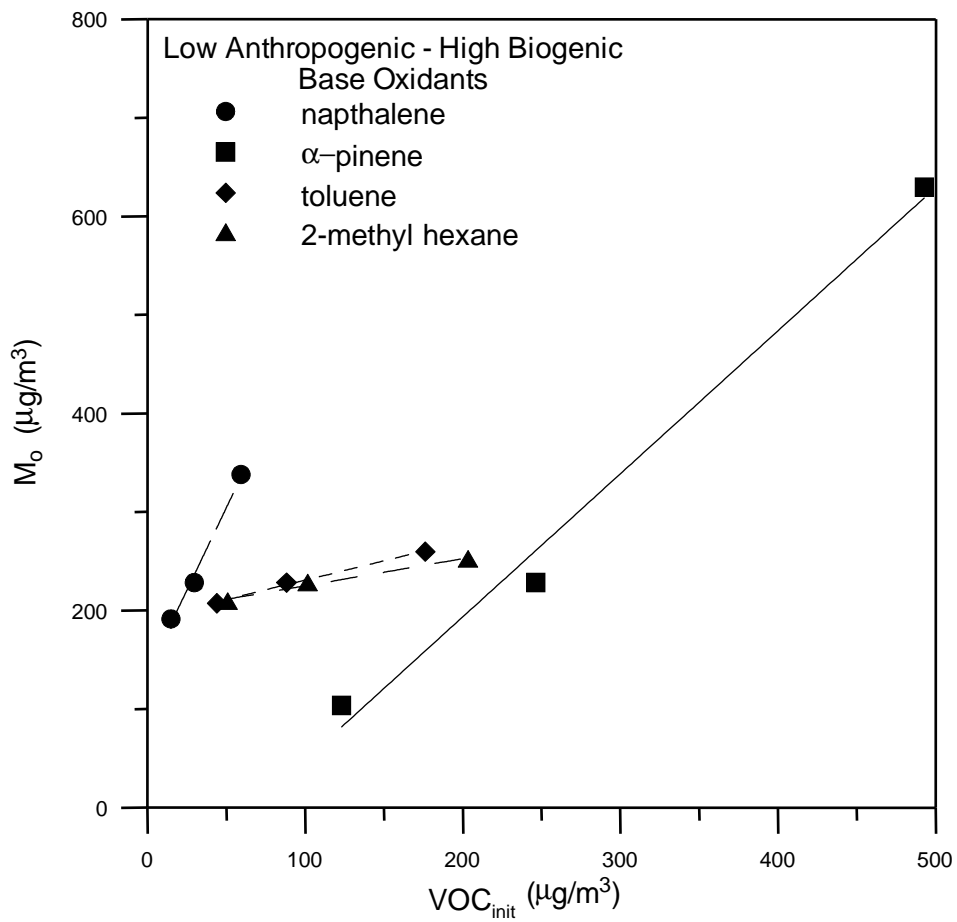


Figure 13. Low Anth VOC- High Bio VOC - Base Ox (Case 8) sensitivity plots of the final organic aerosol mass M_o vs. one initial VOC concentration (slope = θ).

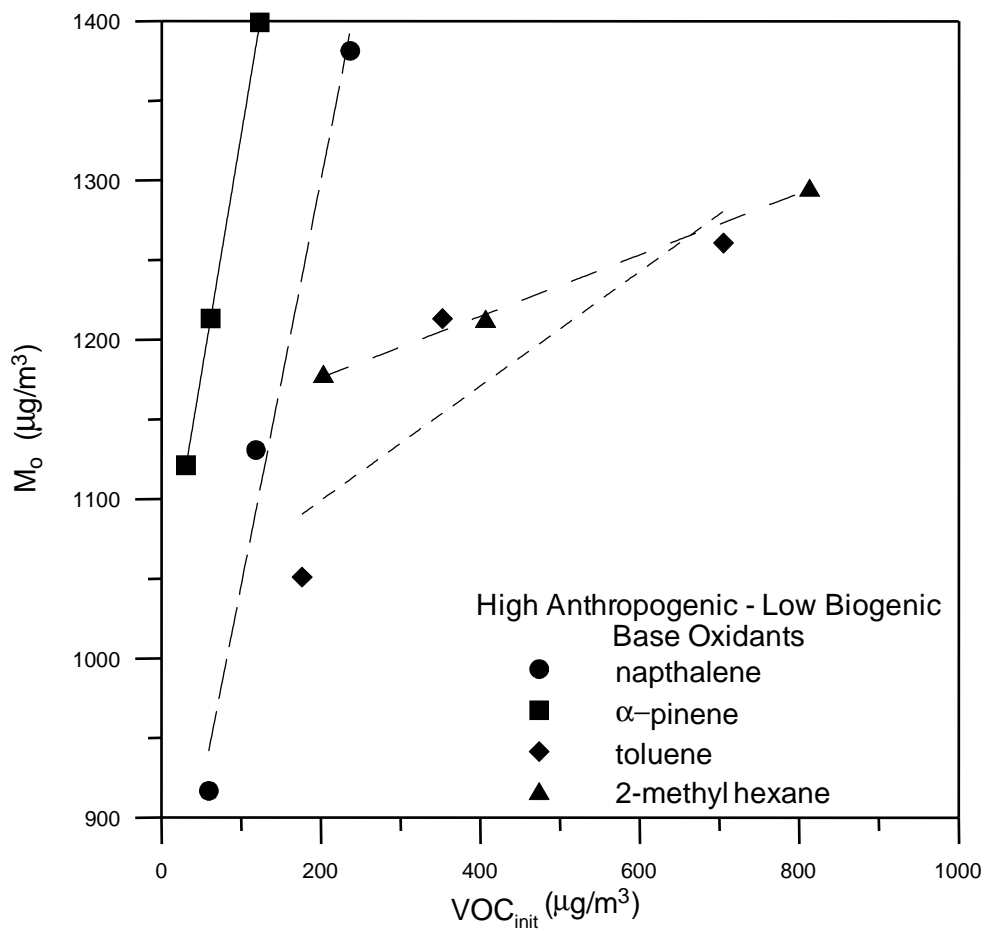


Figure 14. High Anth VOC- Low Bio VOC - Base Ox (Case 9) sensitivity plots of the final organic aerosol mass M_o vs. one initial VOC concentration (slope = θ).

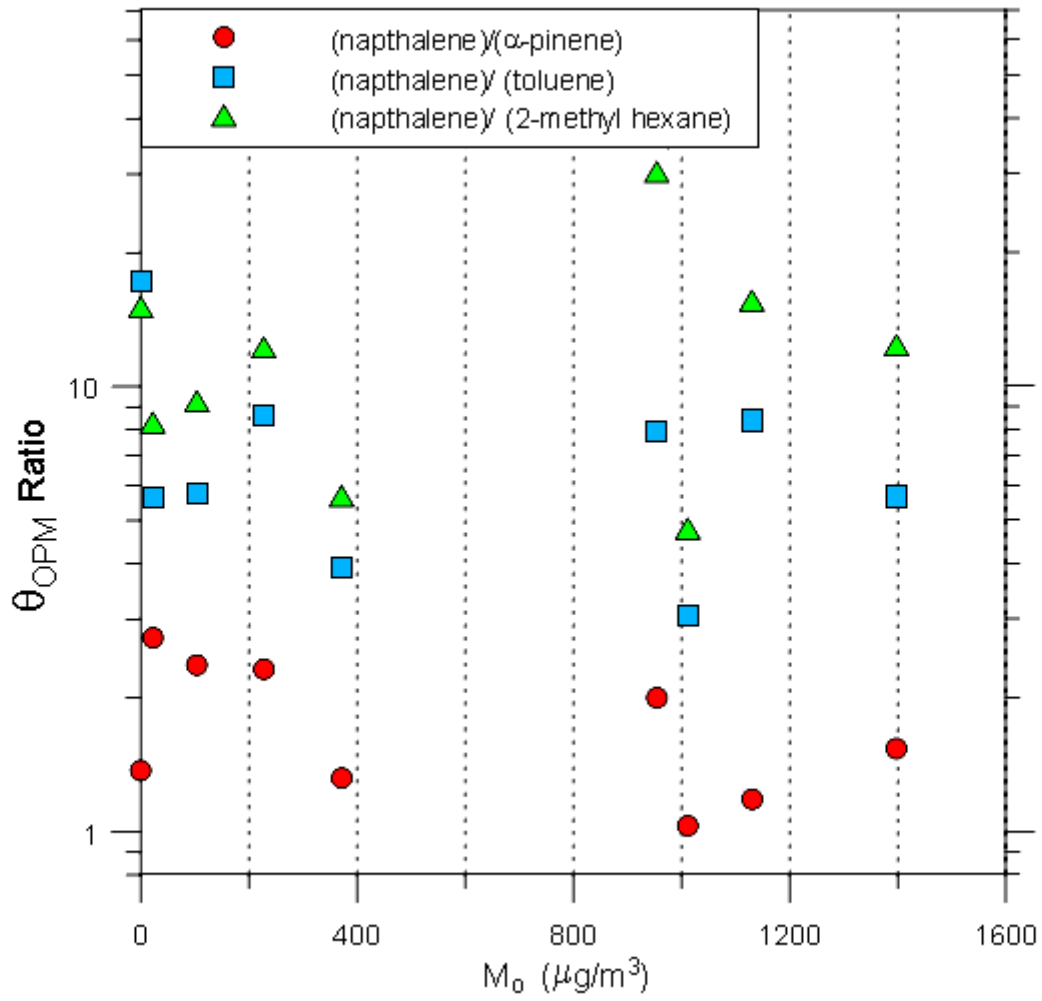


Figure 15. θ Ratios for naphthalene to α -pinene, naphthalene to toluene, and naphthalene to 2-methyl hexane vs. M_o for the study cases.

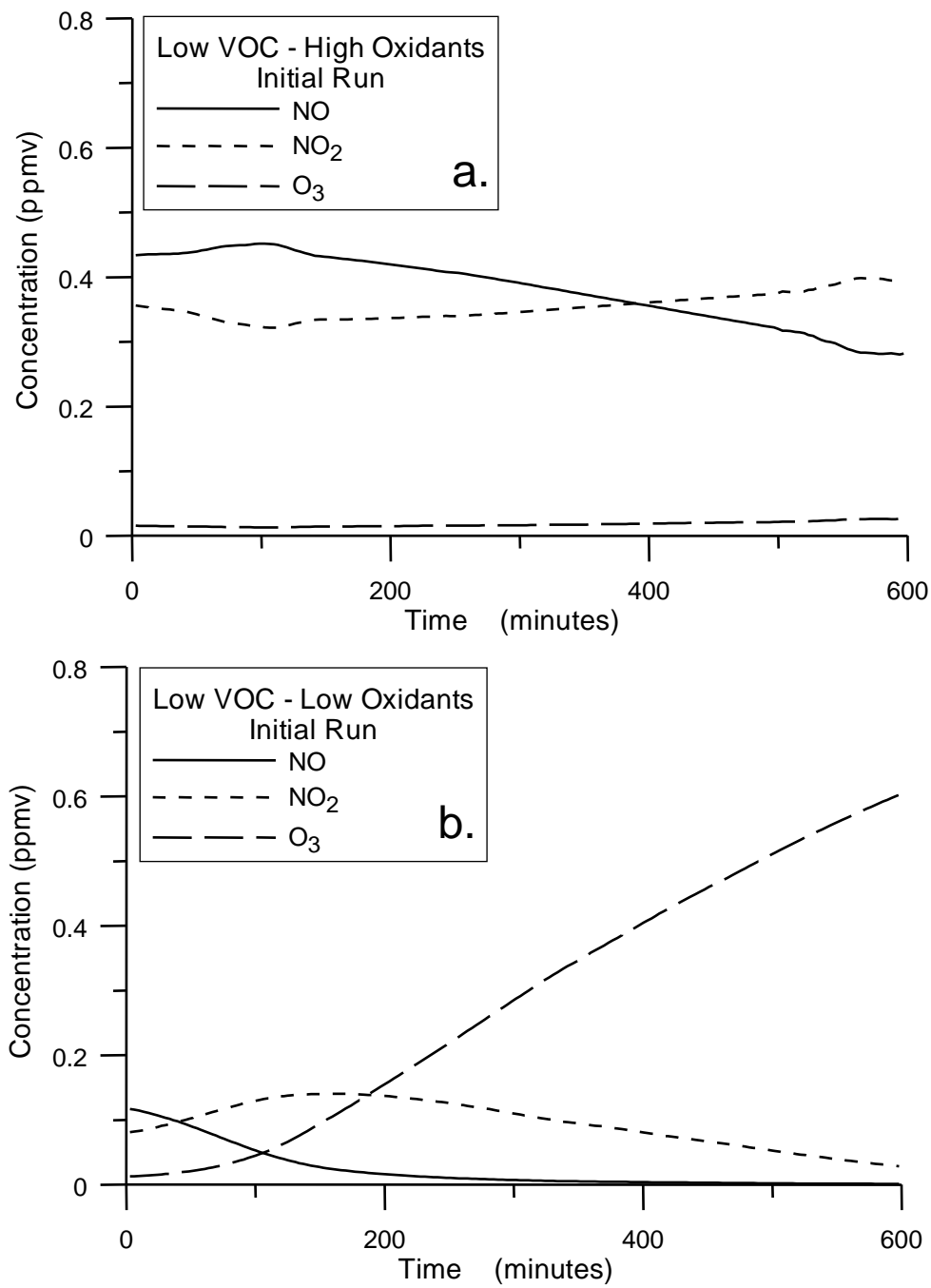


Figure 16. Plot of the time series of NO, NO₂, and O₃ concentrations calculated by OPMBOX for: a. Low VOC- High Oxidant Case (6) (top panel); and b. Low VOC – Low Oxidant Case (7) (bottom panel).

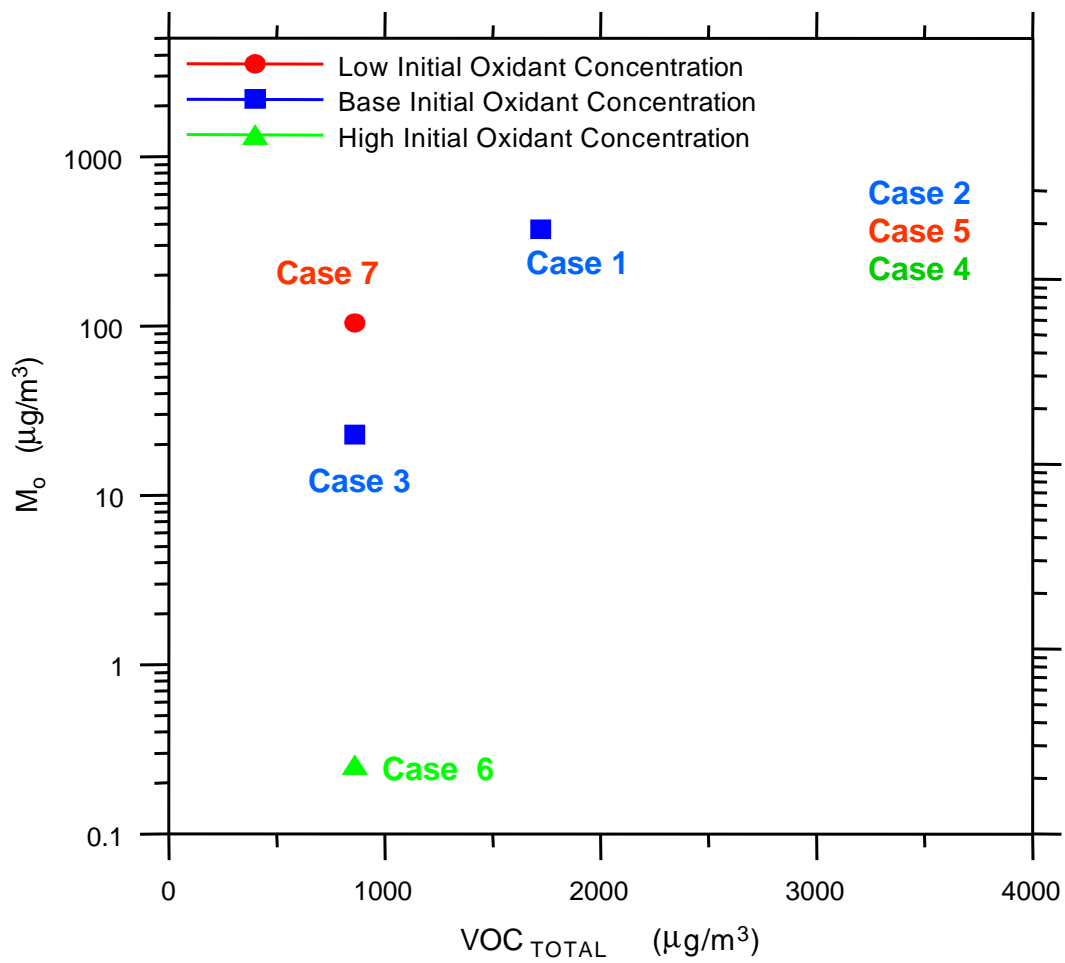


Figure 17. Plot of the organic particulate mass concentration M_o calculated using OPMBOX as a function of total mass of initial parent VOC (VOC_{TOTAL}) for the three different initial Ox levels.

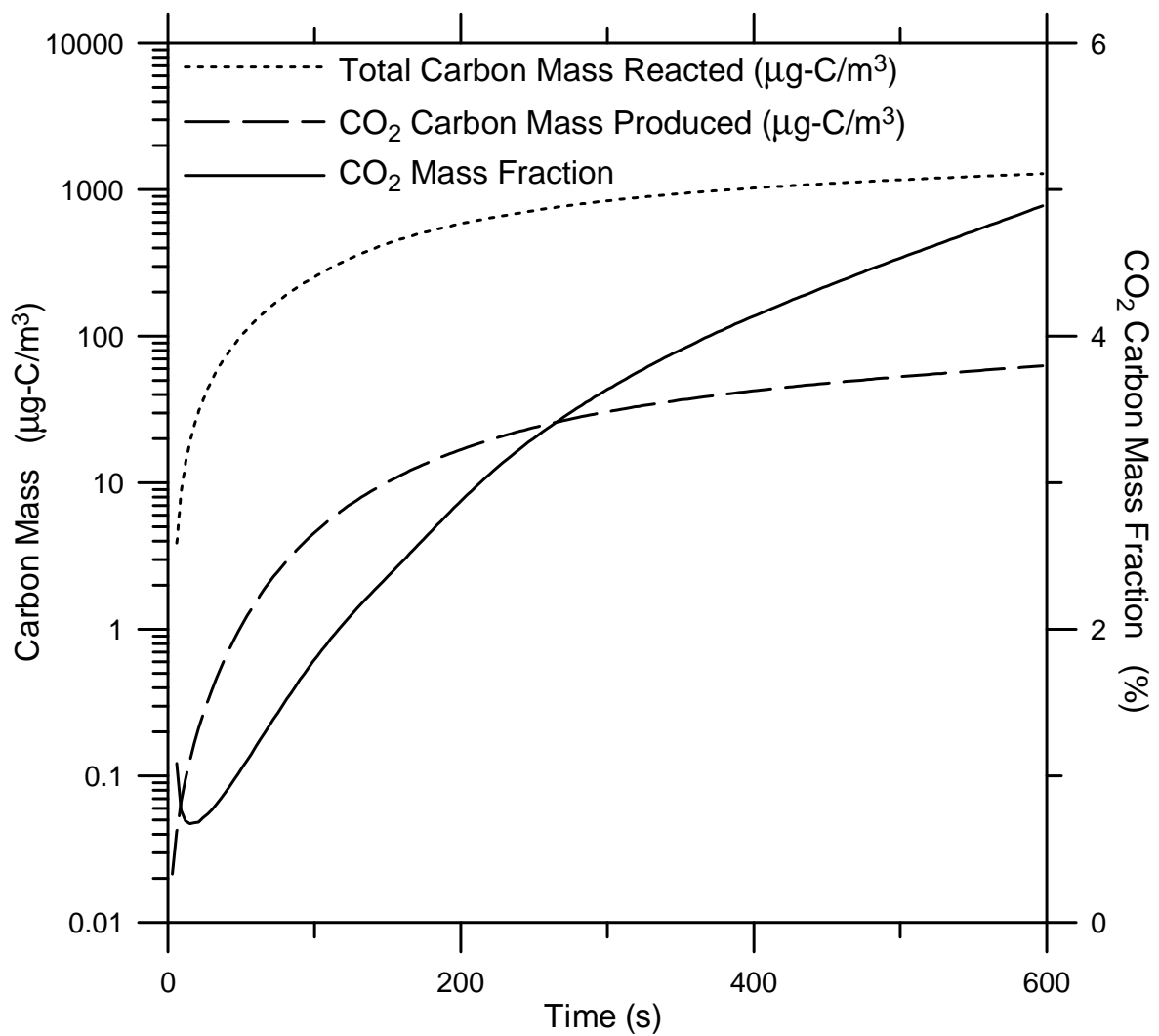


Figure 18. Plot of time evolution of the total carbon mass reacted for the Base Case scenario plotted along with the carbon mass of CO_2 produced. Also shown is the fraction (in terms of per cent) of the total mass of carbon reacted that has been converted to CO_2 .